UPPSALA
UNIVERSITET

Digital Comprehensive Summaries of Uppsala Dissertations from the Faculty of Science and Technology 2047

Studies of Topological Superconductors via Defects

OLADUNJOYE AWOGA

ACTA
UNIVERSITATIS
UPSALIENSIS
UPPSALA
2021

ISSN 1651-6214
ISBN 978-91-513-1219-4
urn:nbn:se:uu:diva-440982

Dissertation presented at Uppsala University to be publicly examined in Häggsalen, Ångströmlaboratoriet, Lägerhyddsvägen 1, Uppsala, Friday, 11 June 2021 at 13:15 for the degree of Doctor of Philosophy. The examination will be conducted in English. Faculty examiner: Professor Pascal Simon (University Paris Saclay).

Abstract

Awoga, O. 2021. Studies of Topological Superconductors via Defects. *Digital Comprehensive Summaries of Uppsala Dissertations from the Faculty of Science and Technology* 2047. 72 pp. Uppsala: Acta Universitatis Upsaliensis. ISBN 978-91-513-1219-4.

Defects from impurities, edges, junctions or domain walls have local detrimental effects on the superconducting state. Defects are also important in topological superconductors, and useful in studying the properties of the superconducting order parameter. In the former case, gapless edge states appear as a consequence of the bulk-edge correspondence, which relates the edge states to the change in bulk topological invariants across the edge. In the latter case impurity scattering of electrons modifies the density of states locally and may (or not) lead to the appearance of subgap states depending on the nature of the impurity and the superconductor. Due to these telltale effects of defects in topological superconductors, this Thesis uses defects to probe topological superconductors. The studies are divided into two parts. In the first part Majorana bound states at the ends of one-dimensional topological superconductors are studied. The Majorana bound states at the ends of magnetic chains are found very stable in a disordered superconducting medium, as long as the superconducting order parameter does not vanish locally. Also junction formed in a nanowire in proximity to two superconductors is found to give rise spontaneously to trivial zero-energy states that imitate Majorana bound states, due to finite size effect of the superconductors. However, there is a sign reversal in the supercurrent when trivial zero-energy states are present at the junction, as magnetic field is tuned, whereas the supercur-rent does not exhibit such sign reversal when Majorana bound states are present at the junction. Thus, supercurrent serves as a tool for distinguishing between Majorana bound states and trivial zero-energy states. The second part is devoted to unconventional and topological superconduc-tivity in graphene. Domain wall states formed between topological chiral $d_{x^2-y^2} \pm id_{xy}$-wave states on the honeycomb lattice are studied. The results find four domain wall states and that domain wall configurations with the lowest width in the order parameter is favorable over other configurations. Finally, by using a single potential impurity spin-singlet gap symmetries of superconducting graphene are explored. Investigation of the subgap states, due to the potential impurity, of each superconducting state and their corresponding quasi-particle interference shows that superconducting states of graphene can be identified by defects.

Oladunjoye Awoga, Department of Physics and Astronomy, Materials Theory, Quantum Matter Theory, Box 516, Uppsala University, SE-751 20 Uppsala, Sweden.

ISSN 1651-6214
ISBN 978-91-513-1219-4
urn:nbn:se:uu:diva-440982 (http://urn.kb.se/resolve?urn=urn:nbn:se:uu:diva-440982)

To everyone

List of papers

This thesis is based on the following papers, which are referred to in the text by their Roman numerals.

I Disorder robustness and protection of Majorana bound states in ferromagnetic chains on conventional superconductors.
Oladunjoye A. Awoga, Kristofer Björnson, and Annica M. Black-Schaffer
Phys. Rev. B 95, 184511 (2017)

II Supercurrent detection of topologically trivial zero-energy states in nanowire junctions
Oladunjoye A. Awoga, Jorge Cayao, and Annica M. Black-Schaffer
Phys. Rev. Lett, 123, 117001 (2019)

III Domain walls in a chiral d-wave superconductor on the honeycomb lattice.
Oladunjoye A. Awoga, Adrien Bouhon, and Annica M. Black-Schaffer
Phys. Rev. B 96, 014521 (2017)

IV Probing unconventional superconductivity in proximitized graphene by impurity scattering.
Oladunjoye A. Awoga, and Annica M. Black-Schaffer
Phys. Rev. B 97, 214515 (2018)

Reprints were made with permission from the publishers.

Author's contribution to the papers

I was responsible for all calculations and preparation of the figures that lead to the results presented in all the papers. I participated in the discussion of the results, interpretation of results, and writing of the papers. I wrote the codes, using mainly MATLAB for both self-consistent and nonself-consistent calculations, for all numerical calculations of Papers II and III. I also wrote MATLAB codes for the calculations of the first part of Paper I where it was necessary to use large lattice size in order to carry out simulations with experimentally realistic parameters. I used software packages for the self-consistent calculations in the second part of Paper I, and the Chebyshev polynomial calculations in Paper IV.

Contents

1. Introduction

Superconductors are materials that conduct electric current, often at temperatures close to absolute zero, with zero resistance [1]. In a superconductor bound states of electron pairs, called Cooper-pair [2], are formed. These Cooper pairs are the carriers of dissipationless supercurrent in the superconducting phase. Below a certain temperature, called the critical temperature, T_c, Cooper pairs form a condensate known as the superconducting phase. The mechanism of pairing of the electrons into Cooper pairs characterizes the superconducting state. In the simple conventional form, the interaction between the electrons in the Cooper pair is phonon-mediated and the pairing of electrons in the superconducting state is isotropic in momentum [3].

Interestingly, it has been shown that electron pairing can also be anisotropic in momentum space. This type of pairing leads to unconventional superconductivity. Unconventional superconductivity was first discovered in heavy fermion compounds [4] at $T_c \approx 0.5$ K, and later in the cuprates with $T_c \approx 135$ K [5], which led to renewed interests in unconventional superconductors. Intense experimental and theoretical efforts has led to the discovery many unconventional superconductors that so far are not well understood [6, 7]. Most unconventional superconductors have layered and complicated structures which contributes to the challenge of pinning down the mechanism for unconventional superconductivity in the materials. For a better understanding of unconventional superconductivity, it might be necessary to study other materials, with relatively simpler structure, that can host unconventional superconductivity.

A candidate material is graphene. When graphene was discovered, physicists were dazzled by its exotic transport properties [8]. At the same time the community was disappointed by the lack of intrinsic superconductivity in graphene. Graphene has a linear low energy dispersion relation which forms a cone in reciprocal space, at the corners of the Brillouin zone. The tip of the cone, called Dirac point or node, coincides with the Fermi energy [9, 10]. The implication of this is that there is no density of states at the Fermi energy and thus no electrons to form Cooper pairs, since pairing of electrons occurs in the vicinity of the Fermi energy. Thus, the Dirac point at the Fermi surface in graphene inhibits superconductivity. However, theoretical studies have suggested that graphene doped close to the van Hove singularity, far away from the Dirac point in energy, will allow for nontrivial superconducting states [11, 12, 13].[1] Therefore, experimental research activities have been on

[1] Such large doping of graphene was impossible until two years ago [14, 15].

efforts to switch on superconductivity in graphene by coupling graphene to a superconductor, a process known as proximity effect. There have been reports of observation of conventional [16, 17] and unconventional [18, **?**, 19] superconductivity in graphene in scanning tunneling spectroscopy experiments.

Superconductivity in graphene is still under investigation. Theory shows that the graphene lattice symmetry allows for different types of superconducting states [12, 20] and it is difficult to know which of the superconducting states is observed in a spectroscopy experiment. The reason for this difficulty is because many of the superconducting states in graphene have similar density of states, especially when doping is low. The problem can also occur at large doping if the scanning tunneling spectroscopy lacks resolution power to clearly distinguish between fully gapped and nodal superconducting states. However, it is known that point defects or impurities have local effects in superconductors and can lead to the emergence of low-energy states within the superconducting gap depending on nature of the impurity and superconductor. [21] Also, the quasi-particle scattering leaves trails in the superconductor. More specifically, a potential impurity distinguishes between conventional and unconventional superconductors: no effect on the former [22] but creates bound states (if the superconductor is fully gapped) or virtual subgap states (if the superconductor is nodal) in the latter [21]. By exploiting the properties of a single potential impurity in superconducting graphene this Thesis shows that it is possible to unambiguously ascertain the gap symmetries of the superconducting state in graphene [23], see Paper IV.

An exotic family of unconventional superconductors with nontrivial topology also exist. Such superconductors are termed topological superconductors [24, 25, 26]. Topology is a mathematical concept for the classification of objects according to their shapes. Objects with different shapes can only be continuously deformed into each other if they belong to the same topological class and are said to remain unchanged under continuous deformation. Similarly, topological superconductors have unchanged properties even when parameters of the system change. Generally, the unchanged property of the system during a continuous deformation is called topological invariant and it is nonvanishing for a topological system. While a topological invariant is a mathematical concept, in condensed matter physics it is also connected to the number of edge states of a topological superconductor through the bulk-edge correspondence [27, 28, 29, 30]. Topological superconductors host gapless states at edges and domain walls [27, 31]. The bulk-edge correspondence states that the number of edge modes at the boundary between two topologically distinct systems is equal to the difference of their topological invariants. By studying domain walls states in topological chiral $d-$wave superconducting states in graphene are studied [31], theis Thesis shows that there are four domain wall states irrespective of domain wall orientation, in agreement with the bulk-edge correspondence. Also, the width of the domain wall follows a universal inverse law, irrespective of parameters, see Paper III.

Some topological superconductors have been theorized to host zero-energy states called Majorana bound states,[2] which are particles that are their own antiparticles, at their boundaries. Unfortunately, topological superconductors with Majorana bound state have not been found. Physicists have, however, found several ingenious ways to engineer a particular topological superconductor hosting Majorana bound state, and have reported signatures of Majorana bound states [32, 33]. There are ongoing debates on whether Majorana bound states have actually be seen in the experiments. This difference of opinion is due to mismatch between theory and experimental data, which suggests the possibility that topologically trivial (nontopological) zero-energy states can appear in experiemtns. For instance, chemical potential inhomogeneity can introduce trivial zero-energy subgap states in superconductors [34, 35, 36], and these trivial zero-energy states can also lead to quantized conductance, a property initially attributed to Majorana bound states [37]. This brings into question the role of disorder, finite size effects, and other parameters of the materials, used in engineering the topological superconductor, and more importantly how to differentiate between trivial zero-energy levels and topological Majorana bound states. This Thesis contribute to the field of topological superconductors by showing that Majorana bound states are robust against disorder [38], see Paper I. The Thesis also shows that spontaneous quantum dot levels with zero energy can appear in experiments and proposes supercurrent as a tool to distinguish between these trivial zero-energy states and Majorana bound states [39], see Paper II.

Contributions of this Thesis

In this Thesis different topological superconductors are studied. The studies are carried out by introducing defects (disorder, junctions, domain walls, and potential impurities) into the superconductor and then study the subgap states of the superconductors. Apart from breaking translation invariance, electrons are scattered at defects causing changes in the local density of states around the defect points. This in turn influence the superconducting order parameter. These can give rise to gapless states, or not, depending on the nature of the superconductor.

The contributions of this Thesis are as follows:

Paper I: Majorana bound states are theorized to be robust against local perturbations due to their non-Abelian nature [40, 41]. But, it is not clear if stable Majorana fermions can exist in a disordered medium in the

[2] In condensed matter literature distinction between Majorana fermions, Majorana zero modes, and Majorana bound states is not clear as they are used interchangeably. However, in the current context these Majoranas are quasi-particles. Thus, they are different from the Majorana fermion in particle physics, which are true particle. In this Thesis, the term Majorana bound states is used.

first place. Furthermore, it was shown that Majorana bound states at ends of nanowires proximitized with conventional superconductors are susceptible to disorder in the bulk of the superconductor especially in the strong coupling regime, suggesting that the superconductor must be clean [42, 43]. Paper I in this Thesis shows that Majorana bound states at the ends 1D topological superconductor, formed by a magnetic chain in a spin-orbit coupled superconductor, are very robust and stable against disorder, as long as superconductivity is not destroyed.

Paper II: Currently, there is no consensus on whether Majorana bound states have been observed or not. This is due to the fact that trivial zero-energy levels can form due to chemical potential inhomogeneity and other sources. Such trivial zero-energy level also produces a zero-bias conductance peak, the same measured signature of Majorana bound states, in experiments. Two important questions are (1) can an *unintended* trivial zero-energy state appear in an experiment designed to create Majorana bound states? And (2) if there is indeed trivial zero-energy level in an experiment, how can one distinguish between trivial zero-energy state and topological Majorana bound states? There have been several proposals for the solution of the second question [44, 45, 39, 46, 47, 48, **?**]. Paper II in this Thesis shows that trivial zero-energy levels can appear spontaneously in junctions of a nanowire strongly coupled to two superconductors. By merely tuning the size of the superconductors the system can move in and out of the trivial zero energy regime. Furthermore, Paper II show that supercurrent through the junction when the trivial zero-energy levels are present exhibits a sign reversal as magnetic field is tuned whereas such sign reversal is not observed in the topological phase when Majorana bound states are present. Thus, Paper II proposes supercurrent as a potential tool for distinguishing between trivial zero-energy levels and Majorana bound states in experiments.

Paper III: It has been theorized that heavily doped graphene and generally honeycomb lattice materials can condense into a topological chiral d-wave superconducting state [20, 13, 12], which is a complex mixture of two different pair symmetry with d-orbital angular momentum. Paper III in this Thesis shows that domain wall states of the topological chiral d-wave state in superconducting graphene can be used as evidence for the existence of chiral d-wave superconducting state on the honeycomb lattice. Creating a domain wall between the $d_{x^2-y^2}+id_{xy}-$wave state with topological invariant $N=+2$ and the $d_{x^2-y^2}-id_{xy}-$wave state with topological invariant $N=-2$, the results show that there are four domain wall states irrespective of domain wall orientation, in agreement with the bulk-edge correspondence. Paper III also shows that while the favored domain wall direction depends on doping and phase difference across the domain wall, the system generally chooses domain walls with the smallest width, set by the suppression of the order parameter. Remark-

ably, despite the sensitivity of the favored domain wall orientation to several parameters, the domain wall width behavior as a function of the bulk superconducting order parameter follows an inverse law, which is universal. For all variation of parameters, the plot of the width of the favored domain wall against the bulk superconducting order parameter always falls on a single curve.

Paper IV: An STS experiment on low doped graphene sheet proximitized with a cuprate superconductor reported the presence of a superconducting gap in the graphene sheet [18]. Due to the V-shape of the spectral gap, the induced superconductivity was attributed to $p-$wave pairing. However, in theory, the myriad of superconducting states allowed by the honeycomb lattice of graphene, some with similar density of states, makes it difficult to identify the superconducting state through STS experiments, especially when resolution is poor and/or when doping is low. Paper IV in this Thesis uses a single nonmagnetic impurity to create subgap states in superconducting graphene and the results show that the subgap states, and accompanying quasi-particle interference, can reveal the type of superconducting symmetries. This study proposes that by including a potential impurity in superconducting graphene in STS the symmetry of the superconducting in graphene can be determined.

All the above studies have been carried out numerically using a tight-binding approach on either square or honeycomb lattice.

Part I:
Background

In this part, basics of the theory of superconductivity relevant to this Thesis are discussed. Also discussed are the numerical methods used to simulate the systems studied in this Thesis.

2. Superconductivity

2.1 Overview

In 1911 Kamerlingh Onnes found that the resistance of mercury jumps to zero at temperatures lower than 4.2 K [49]. It was later found that this (low temperature) zero resistance is not peculiar to mercury but is exhibited by many elements. However, the critical temperature, T_c, at which the resistance becomes zero varies from element to element. This phenomenon was called superconductivity. When a material becomes superconducting it develops an order parameter, which is finite below T_c but vanishes above T_c. Zero resistance, that is perfect conductivity, is not the only telltale signature of superconductivity. Another feature of superconductivity is the so-called Meissner effect [50]: a superconductor expels magnet field from its core thereby exhibiting perfect diamagnetism.

At the early stages, while the community searched for a microscopic theory of superconductivity, many of the properties of superconductivity were predicted from phenomenological theories. In 1935, the London brothers studied the electrodynamics of the superconducting phase and derived the London equations which explain the Meissner effect in a superconductor [51]. About twenty years later, Pippard generalized the London equations and derived the coherence length of the superconducting phase [52, 53]. In 1950, by assuming a complex wave function and taking it as the order parameter of the superconducting phase, the Ginzburg-Landau theory was derived by expanding the free energy in powers of the wave function [54]. The Ginzburg-Landau theory is a macroscopic theory which predicts critical fields and spatial inhomogeneity of the order parameter. Despite the success of phenomenological theories the mechanism of superconductivity was not understood because there were still open questions such as the microscopic constituent of a superconductor.

The celebrated Bardeen-Cooper-Schrieffer (BCS) theory, which gives microscopic explanation of superconductivity came in 1957. Noting that in the superconducting state: (1) there is an *attractive electron-phonon interaction* whose strength supersedes the repulsive Coulomb interaction [55, 56] and (2) a pair of electrons close to Fermi energy with this attractive interaction forms a bound electron pair called *Cooper pair* [2]. Below T_c the Cooper pairs condense into a superconducting phase. (3) Taking the superconducting ground state as a coherent state of Cooper pairs, BCS introduced an ansatz wave function and formed the microscopic theory [57, 58]. With the assumption that the interaction and spatial dependence of the Cooper pair are isotropic, BCS

predicted correctly all properties of superconductivity obtained from experimental data as of then. One of the ultimate triumph of the BCS theory is the prediction of the energy gap, the minimum energy required to break a Cooper pair, which could not be explained by phenomenological theories. The assumption of spatially isotropic Cooper pairs worked because during that period only elemental superconductors were discovered and the assumption is valid for these type of superconductors. Today, these type of superconductors are called *conventional* superconductors.

With the BCS theory, superconductivity seemed to be understood and thus a closed chapter. This view changed when superconductors with anisotropic momentum dependent Cooper pair arrived on the scene. These superconductors are called *unconventional* superconductors. Unconventional superconductivity was first discovered in a heavy fermion material in 1979 by Steglich and coworkers [4]. But due to the low $T_c \approx 0.5$ K of the superconductors, coupled with the fact that they were not understood, the discovery did not generate much attention. In 1986, unconventional superconductivity was discovered in cuprates by Bednordz and Müller [5] and this time with $T_c \approx 135$ K, which is a very high T_c compared to other known superconductors as of then. For this reason they are termed High Temperature Superconductors. The discovery of cuprates led to intensified efforts in search for unconventional superconductivity in several materials including heavy fermions materials [59, 7], graphene [11, 13, 12], twisted bilayer graphene [60] and other materials [6]. To treat unconventional superconductivity the original BCS theory has been extended to what is now called the *generalized BCS theory*. The generalized BCS theory removes the restriction that the attractive interaction responsible for Cooper pairs is phonon-mediated, thus allowing for pure electron-electron interaction. For the electrons to overcome the repulsive Coulomb interaction between them, the Cooper pair would develop nontrivial spatial dependence, see section 2.3.1.

In the presence of quantum mechanical symmetries superconductors can develop special geometrical properties. When this happens the superconductors are said to be topological [24, 40]. These superconductors host Majorana bound states, which are condensed matter physics versions of the elusive Majorana fermions in particle physics [61]. Majorana bound states have non-Abelian properties that protects them robust against local perturbation, and this makes Majorana bound states suitable candidate for qubits in topological quantum computing. Since the first experiment which reported "signatures" of Majorana bound states in 2012 [32], the search for Majorana bound states and topological superconductivity has been very active.

Although, superconductivity is ubiquitous among elemental metals and many materials, naturally occurring topological superconductors are rare and many unconventional superconductors are complex compounds. Thus, studying the latter is complicated by material composition. However, it is possible to propel nonsuperconducting materials, with no intrinsic superconductivity, towards

superconductivity by placing them next to a superconductor. Superconducting correlations are induced in the nonsuperconducting through proximity effect. Here, Cooper pairs leak from the superconductor, assuming a good interface, into the nonsuperconducting material which then becomes superconducting [62]. This is an interesting and viable route to achieve, and study, unconventional and topological superconductivity, with intense activity lately [63].

After more than 100 years since its discovery, superconductivity is still an exciting field and, even more fascinating, a growing field as more materials with nontrivial superconducting phase are being discovered and many created through proximity effect. Also, there are still challenging but crucial problems such as explaining the mechanism of superconductivity in cuprates, pinning down the nature of superconductivity in the enigmatic Sr_2RuO_4, determining superconducting symmetries of graphene systems, finding probe for unambiguous detection of MBS, just to mention a few.

This Thesis meets the challenges of superconductivity in two aspects using defects as a probe. In one part, superconductivity in graphene is studied in order to understand its nature as well as give theoretical predictions. In the other part, Majorana bound states at the ends one-dimensional topological superconductors are investigated using defects such as potential disorder and junctions, in order to determine the stability of Majorana bound states and also predict a decisive experimental probe for their detection.

The rest of this chapter is devoted to the basics of superconductivity. The BCS theory, Bogoliubov-de Gennes formalism and proximity effect are briefly discussed vis-á-vis papers in this Thesis.

2.2 Basics of superconductivity

In this section, basic concepts of superconductivity relevant to the Thesis are discussed. Further technical details can be found in standard textbooks [1, 3, 64].

2.2.1 Generalized BCS Hamiltonian

This Thesis is focused on unconventional superconductivity so the starting point is the generalized BCS Hamiltonian which incorporates superconducting states with nontrivial spatially dependent order parameters.

Consider a material with underlying lattice system. The generalized BCS Hamiltonian in real space is given by

$$H = \sum_{ij\alpha\beta} h^0_{i\alpha,j\beta} c^\dagger_{i\alpha} c_{j\beta} + \frac{1}{2} \sum_{ij\alpha\beta\delta\gamma} V^{\alpha\beta\delta\gamma}_{ij} c^\dagger_{i\alpha} c^\dagger_{j\beta} c_{j\delta} c_{i\gamma} \tag{2.1}$$

where i, j label sites and other quantum numbers and Greek letters label spin. The first term is the normal state Hamiltonian of the system while the second

term contains interaction between electrons, where a factor of $1/2$ has been included to avoid double counting. Here, $V_{ij}^{\alpha\beta\delta\gamma} = \langle i\alpha, j\beta|\hat{V}|j\delta, i\gamma\rangle$ is the interaction matrix element. Throughout this Thesis $V_{ij}^{\alpha\beta\delta\gamma}$ is assumed to be constant between paired sites. Discussion on the origin of the interaction or mechanism by which it gives rise to superconductivity is postponed to later sections. The reasons for shelving the discussion on interaction to later sections are (1) explicit knowledge of $V_{ij}^{\alpha\beta\delta\gamma}$ is not necessary for now and (2) there are constraints on $V_{ij}^{\alpha\beta\delta\gamma}$, which are yet to be discussed, that will help making deductions about the origin of the interaction easier. The operator $c_{i\alpha}^{\dagger}(c_{i\alpha})$ creates (destroys) an electron of spin α at site $i = i(i_x, i_y, i_z)$. The operators obey fermionic anticommutation relations,

$$\{c_{i\alpha}^{\dagger}, c_{j\beta}\} = \delta_{ij}\delta_{\alpha\beta}, \qquad \{c_{i\alpha}, c_{j\beta}\} = \{c_{i\alpha}^{\dagger}, c_{j\beta}^{\dagger}\} = 0 \tag{2.2}$$

The single particle noninteracting, first term in Eq. (**??**), is quadratic in the c operators. However, the interaction term is quartic making Eq. (2.1) difficult to solve. To make the Hamiltonian more tractable it will be decomposed using the mean-field approach.

2.2.2 Mean-field decomposition BCS Hamiltonian

One can collate the 2×2 identity matrix and the Pauli matrices as $\sigma^{\eta} = \{\sigma^0, \sigma^x, \sigma^y, \sigma^z\}$. Using this abridged notation to introduce the matrices

$$\bar{\sigma}^{\eta} = i\sigma^{\eta}\sigma^{y}, \qquad \text{with,} \qquad \frac{1}{2}\sum_{\eta}[\bar{\sigma}^{\eta}]_{\alpha\beta}^{\dagger}[\bar{\sigma}^{\eta}]_{\delta\gamma} = \delta_{\alpha\gamma}\delta_{\beta\delta} \tag{2.3}$$

in the interacting part of Eq. (2.1) and then decomposing in particle-particle channel by writing $cc \longrightarrow (cc - \langle cc\rangle) + \langle cc\rangle$ with the assumption that fluctuations around the average is negligible and keeping only first order in the fluctuations, one obtains the mean-field Hamiltonian as[1]

$$\begin{aligned} H_{\mathrm{MF}} = &\sum_{ij\alpha\beta} h^0_{i\alpha,j\beta} c^{\dagger}_{i\alpha} c_{j\beta} + \sum_{ij\alpha\beta\eta} \Delta^{\eta}_{ji} c^{\dagger}_{i\alpha} [\bar{\sigma}^{\eta}]^{\dagger}_{\alpha\beta} c^{\dagger}_{j\beta} + \mathrm{H.c} \\ &- \sum_{ij} \left(\Delta^{\eta}_{ij}\right)^{\dagger} \left(\Gamma^{\eta}_{ij}\right)^{-1} \Delta^{\eta}_{ji}, \end{aligned} \tag{2.4}$$

where

$$\Delta^{\eta}_{ji} = \frac{1}{2}\sum_{\delta\gamma}\Gamma^{\eta}_{ij}\langle c_{j\delta}[\overline{\sigma}^{\eta}]_{\delta\gamma} c_{i\gamma}\rangle = \sum_{\delta\gamma}\Gamma^{\eta}_{ij} F^{\eta}_{j\delta,i\gamma}, \tag{2.5}$$

$$F^{\eta}_{j\delta,i\gamma} = \langle c_{j\delta}[\overline{\sigma}^{\eta}]_{\delta\gamma} c_{i\gamma}\rangle,$$

[1] Similar decomposition can be carried out in particle-hole channel by writing $c^{\dagger}c \longrightarrow \left(c^{\dagger}c - \langle c^{\dagger}c\rangle\right) + \langle c^{\dagger}c\rangle$. In this Thesis the focus is on superconductivity only.

$\Gamma^{\eta}_{ij} = \frac{1}{2}\sum_{\alpha\gamma} V^{\alpha\beta\delta\gamma}_{ij}\sigma^{\eta}_{\alpha\beta}\sigma^{\eta}_{\delta\gamma}$ is the mean-field decomposed interaction in channel η and H.c. implies Hermitian conjugate. Here, $\eta = 0\big(\eta = x,y,z\big)$ denotes spin-singlet (spin-triplet). The last term in H_{MF}, Eq. (2.4), is a constant that is not important for the rest of this chapter so it is dropped. Note that this constant term is important in some calculations, such as the free energy, and has to be included when necessary.

The quantity Δ^{η}_{ji} is called the *gap function* or *order parameter* of the superconducting state and can be calculated from the *self-consistent equation*, Eq. (2.5). To elucidate the role of Δ^{η}_{ji} as the superconducting order parameter consider the gauge transformation $U\big(1\big) : c_j \to c_j e^{i\phi}$, where ϕ is an arbitrary space independent phase. The normal state Hamiltonian, that is the first term of H_{MF}, is invariant under this transformation, however, under the same transformation $\Delta^{\eta}_{ji} \to e^{2i\phi}\Delta^{\eta}_{ji}$, see Eq. (2.5). Thus, superconductivity breaks the $U\big(1\big)$ gauge symmetry. But $U\big(1\big)$ is a symmetry of the normal state. Hence, the transition from the normal state to superconducting phase is a *spontaneous symmetry breaking* (SSB) transition: a situation where the normal state has a symmetry that is not present in the ground state. Since Δ^{η}_{ji} breaks a symmetry under which the normal state is invariant, it must be that $\Delta^{\eta}_{ji} = 0$ in the normal state and finite only in the superconducting phase. This is exactly the definition of an order parameter: a quantity that vanish in one phase and become nonvanishing in another phase. The temperature at which the order parameter becomes finite is called the *critical temperature*, T_{c}.

The function $F^{\eta}_{j\delta,i\gamma}$ is called the *pair wave function* of the superconducting state. $F^{\eta}_{j\delta,i\gamma}$ is an expectation value of a pair of electrons. Since $F^{\eta}_{j\delta,i\gamma}$ contains two electrons it must obey the fermion antisymmetrization rule i.e.

$$F^{\eta}_{j\delta,i\gamma} = -F^{\eta}_{i\gamma,j\delta}, \tag{2.6}$$

and it can be factored into spatial and spin components. This implies that spin-singlet superconductors, $\eta = 0$, are even under spatial inversion while the spin-triplet counterparts, $\eta = \{x,y,z\}$, are odd under spatial inversion. Thus, spin-singlet (-triplet) superconductors have $s, d, g, \cdots (p, f, \cdots) -$ orbital symmetries.

The order parameter Δ^{η}_{ji} can be interpreted, from Eq. (2.4), as the amplitude for pair creation while its Hermitian conjugate is the amplitude for pair annihilation. These electron pairs are the so-called Cooper pairs, which are formed just above the Fermi surface [2]. From the self-consistent equation, Eq. (2.5), it obvious that Δ^{η}_{ji} inherits the symmetries of $F^{\eta}_{j\delta,i\gamma}$. Since interaction is assumed to be isotropic in space in this Thesis, one can focus on the order parameter instead of the pair wave function.

The mean-field Hamiltonian is bilinear Eq. (2.4) but not diagonal in the c-operators because of the particle-particle terms. H_{MF} can be diagonalized if the c-operators are rotated to a basis where they are linear combinations of an

operator and its conjugate. This is the approach of the Bogoliubov-de-Gennes formalism which is the subject of next section [1].

2.2.3 Bogoliubov-de Gennes formalism

The effective mean-field Hamiltonian can be made simple by introducing the so-called, Nambu spinor $\Psi_i = \sum_\alpha \left(c_{i\alpha}\ c^\dagger_{i\alpha}\right)$, at site i, which has equally weighted electron and hole components [65]. Ψ obeys the same fermionic anticommutation relations as the c-operators. Introducing the spinor in $H_{\rm MF}$ one obtain

$$H_{\rm MF} = \frac{1}{2}\Psi_i^\dagger \hat{H}_{\rm BdG}\Psi_j, \qquad \text{with} \qquad \hat{H}_{\rm BdG} = \sum_{ij}\begin{pmatrix} \hat{H}_0(i,j) & \hat{\Delta}(i,j) \\ \hat{\Delta}(i,j)^\dagger & -\hat{H}_0(i,j)^T \end{pmatrix} \tag{2.7}$$

where the factor $1/2$ is introduced to avoid double counting since the introduction of Nambu spinor doubles the degree of freedom. The matrices $\hat{H}_0$ and $\hat{\Delta}$ contain matrix elements $h^0_{i\alpha,j\beta}$ and Δ^η_{ji} respectively. The matrix $\hat{H}_{\rm BdG}$ is called Bogoliubov-de-Gennes Hamiltonian, a first quantized Hamiltonian.

Since $\hat{H}_0$ is Hermitian, then $\hat{H}_{\rm BdG}$ is an Hermitian matrix. Thus, there exist an orthonormal basis for which $\hat{H}_{\rm BdG}$ is diagonalized with real eigenvalues. From the structure of $\hat{H}_{\rm BdG}$ and symmetry of $\hat{\Delta}$ one can show that for every eigenvalue E^ν there exist another eigenvalue $-E^\nu$ where $\nu = 1,2,...,4N$. N is number of sites. By merely observing the structure of $\hat{H}_{\rm BdG}$ valuable information on the excitations of a superconductor has been revealed. These excitations, which turn out to be *quasi-particles*, reveal themselves as linear combination of electrons and holes which diagonalize $\hat{H}_{\rm BdG}$.

Excitations in superconductors

In this subsection $H_{\rm MF}$ is diagonalized and the excitations which diagonalizes $\hat{H}_{\rm BdG}$ are obtained. The aim is to gain understand of the superconducting state and its low energy behavior.

Equation (2.4) can be diagonalized by a linear combination of c and $c^\dagger$, i.e. electron-hole combination. A convenient way of introducing such linear combination is through Bogoliubov-Valatin transformation [66, 67], written as

$$c_{i\alpha} = \sum_\nu{}' \left(u^\nu_{i\alpha}\gamma_\nu - s_\alpha v^{*\nu}_{i\bar{\alpha}}\gamma^\dagger_\nu\right), \qquad c^\dagger_{i\alpha} = \sum_\nu{}' \left(u^*_{i\alpha}\gamma^\dagger_n - s_\alpha v^\nu_{i\bar{\alpha}}\gamma^\dagger_\nu\right) \tag{2.8}$$

where prime on the summation sign implies positive energies only and $s_\alpha = -1(+1)$ for spin-up(spin-down). The new operators γ are called *Bogoliubov quasi-particles*. The γ's can be obtained as a linear combination of c and $c^\dagger$ by inverting the transformation. This means that γ and $\gamma^\dagger$ are fermionic and thus obey the same anticommutation relations as the c-operators. By substituting

Eq. (2.8) into Eq. (2.4) the Hamiltonian becomes diagonal, and reads

$$H_{\mathrm{MF}} = \sum_{\nu} E^{\nu} \gamma_{\nu}^{\dagger} \gamma_{\nu} \tag{2.9}$$

By taking commutators $[c_{i\alpha}, H_{\mathrm{MF}}]$ and $[\gamma_{\nu}, H_{\mathrm{MF}}]$ (and same for the conjugate operators), and collecting the coefficient of γ and $\gamma^{\dagger}$ one obtains two sets of equations namely,

$$\begin{aligned} \gamma_{\nu}: \quad & \hat{H}_{\mathrm{BdG}} \psi_i^{\nu} = E^{\nu} \psi_i^{\nu} \\ \gamma_{\nu}^{\dagger}: \quad & \hat{H}_{\mathrm{BdG}} \psi_i^{*\nu} = -E^{\nu} \psi_i^{*\nu} \end{aligned} \tag{2.10}$$

where $\psi_i^{\nu} = \sum_{\alpha} \begin{pmatrix} u_{i\alpha}^{\nu} \\ s_{\alpha} v_{i\alpha}^{\nu} \end{pmatrix}$, $\psi_i^{*\nu} = \sum_{\alpha} \begin{pmatrix} s_{\alpha} v_{i\alpha}^{*\nu} \\ -u_{i\alpha}^{*\nu} \end{pmatrix}$ and $\hat{H}_{\mathrm{BdG}}$ is given in Eq. (2.7).

Several insights into the world of superconductivity are revealed in Eq. (2.10). It is in order to make these observations.

- These are eigenvalue equations implying that by knowing $\hat{H}_{\mathrm{BdG}}$ one can obtain all necessary information about the superconductor by simply diagonalizing $\hat{H}_{\mathrm{BdG}}$.
- For every positive energy state with eigenvalue E^{ν} and eigenvector ψ_i^{ν} there is a negative energy state with eigenvalue $-E^{\nu}$ and eigenvector $\psi_i^{*\nu}$.
- The existence of both negative and positive energy states is an indication of particle-hole symmetry. Denoting particle-hole symmetry operator by[2] $\mathcal{P} = -i\tau^{y} \otimes \tau^{0} K$, where $\tau\,(\sigma)$ and K are, respectively, Pauli matrix in particle-hole (spin) space and the complex conjugate operator, one notes the relationship between negative and positive energy states as

  $$\mathcal{P} \hat{H}_{\mathrm{BdG}} \mathcal{P}^{-1} = -\hat{H}_{\mathrm{BdG}}, \qquad \mathcal{P} \psi_i = \psi_i^{*} \tag{2.11}$$

  Particle-hole symmetry is an inherent property of all superconductors. It comes into light from the introduction of holes through the Nambu spinor.
- From the structure of $\hat{H}_{\mathrm{BdG}}$ it is clear that $\hat{\Delta}$ mixes electrons with holes, thus playing a role akin to a coupling parameter. Hence, it is expected that the spectrum of a superconductor is gapped by Δ and it is symmetric around zero energy, (since for every E^{ν} there is $-E^{\nu}$).
- By collecting the ψ's and $\mathcal{P}\psi$'s in column to form a matrix one obtains the unitary matrix ($\hat{H}_{\mathrm{BdG}}$ is Hermitian) that diagonalizes $\hat{H}_{\mathrm{BdG}}$ as

  $$\hat{U} = \sum_{\alpha} \begin{pmatrix} u_{i\alpha}^{\nu} & s_{\alpha} v_{i\alpha}^{\nu *} \\ s_{\alpha} v_{i\alpha}^{\nu} & -u_{i\alpha}^{\nu *} \end{pmatrix} \tag{2.12}$$

- Inverting the transformation Eq. (2.8) one obtains the γ-operators as a linear combination of electron and holes. Thus superconducting state is

[2] It should be noted that form of the particle-hole operator is basis dependent.

a vacuum state of γ. The $\gamma\left(\gamma^{\dagger}\right)$-operator destroys (creates) one electron and one hole in the condensate.

- Using the anticommutation relation for c- and γ-operators one obtains

$$u^{\nu}_{i\alpha}u^{*\nu}_{j\beta}+v^{*\nu}_{1\alpha}v^{\nu}_{j\beta}=\delta_{ij}\delta_{\alpha\beta} \text{ and } u^{\nu}_{i\alpha}v^{*\nu}_{j\beta}+v^{\nu}_{i}u^{*\nu}_{j\beta}=0,$$

where u and v are the amplitude of electron and hole in the linear combination and are called *coherence factors*.

In this Thesis, $\hat{H}_{\mathrm{BdG}}$ is solved for several systems. Note that $\hat{H}_{\mathrm{BdG}}$ is a large matrix of size $4N\times 4N$ where N is the number of sites. It is not always feasible to carry out direct diagonalization of $\hat{H}_{\mathrm{BdG}}$. Various methods of accessing relevant information of target physics stored in $\hat{H}_{\mathrm{BdG}}$ are discussed in Chapter 4. For systems with conserved spin rotation symmetry $\hat{H}_{\mathrm{BdG}}$ becomes block diagonal and each block has size $2N\times 2N$. In this case it is enough to consider only one of the blocks. This approach reduces the size of the problem.

2.2.4 Homogeneous superconductor

Hitherto, the discussion has been in real space. The BdG Hamiltonian is a large matrix in real space making it difficult to handle analytically. However, for large systems in the absence of defects, the problem is usually simplified by working in momentum space. When a material has translation symmetry, i.e. homogeneous, one usually work in momentum space by using the discrete Fourier transform

$$c_{j\alpha}=\frac{1}{\sqrt{N_k}}\sum_{k}c_{kj\alpha}e^{ik\cdot r_j}, \tag{2.13}$$

where N_k is the number of $k-$points, and $j=\{j,r_j\}$, r_j is position vector and j is a compressed index for other labels including orbitals, sublattice etc.

Using this in the effective Hamiltonian, Eq. (2.4), and writing $r_j=r_i+a$, where a is a vector along the bonds between paired sites, one obtains the momentum space version of Eq. (2.4) as

$$H_{\mathrm{MF}}=\sum_{k\alpha\beta}h^{0}_{\alpha_\beta}(k)c^{\dagger}_{ki\alpha}c_{kj\beta}+\sum_{ijak}\sum_{\alpha\beta\eta}\Delta^{\eta}_{ji,a}c^{\dagger}_{ki\alpha}\left[\bar{\sigma}^{\eta}\right]^{\dagger}_{\alpha\beta}c^{\dagger}_{-kj\beta}e^{ik\cdot a}+\mathrm{H.c.} \tag{2.14}$$

and the gap equation Eq. (2.5) becomes

$$\Delta^{\eta}_{ji,a}=\sum_{k\delta\gamma}\Gamma^{\eta}_{ji}\langle c_{-kj\delta}\left[\bar{\sigma}^{\eta}\right]_{\beta\alpha}c_{ki\gamma}\rangle e^{-ik\cdot a}=\sum_{k\delta\gamma}\Gamma^{\eta}_{ji}F_{\delta\gamma}(k) \tag{2.15}$$

To reiterate, here it is assumed that interactions are momentum independent.

Introducing the Nambu spinor $\Psi_k=\sum_{i\alpha}(c_{ki\alpha}\ c^{\dagger}_{-ki\alpha})^T$ in momentum space one obtains

$$H_{\mathrm{MF}}=\frac{1}{2}\Psi^{\dagger}_{k}\hat{H}_{\mathrm{BdG}}\Psi_k, \qquad \hat{H}_{\mathrm{BdG}}=\begin{pmatrix}\hat{H}_0(k) & \hat{\Delta}(k)\\ \hat{\Delta}^{\dagger}(k) & -\hat{H}^{T}_{0}(-k)\end{pmatrix} \tag{2.16}$$

Similar to the real space version, the Nambu spinor renders the Hamiltonian into a first quantized Hamiltonian $\hat{H}_{\mathrm{BdG}}$, which is a $4L \times 4L$ matrix, L is the total of the abridged index i, which labels sublattices, orbitals, etc. All the features of superconductivity discussed with real space analysis in the last section are unchanged in momentum space. One can show that the momentum space version of particle-hole symmetry of superconductivity is

$$\mathcal{P}\hat{H}_{\mathrm{BdG}}(k)\mathcal{P}^{-1} = -\hat{H}^{T}_{\mathrm{BdG}}(-k), \qquad \text{with } \mathcal{P}\phi_k = \phi^{*}_{-k} \tag{2.17}$$

The particle-hole operator transforms an electron with positive energy and momentum k to a hole with negative energy and momentum $-k$.

The properties of the superconductivity has now been discussed. However, an important question that is yet to be answered is how to predict the transition or critical temperature, T_{c}, of a superconductor. This is discussed in the next section.

2.3 The superconducting order parameter and transition temperature

As explained earlier the system undergoes a phase transition from the normal state to the superconducting phase by developing a superconducting order parameter, Δ, which is zero in the normal phase but become finite just at T_{c}. Just below T_{c} the order parameter, Δ, is small. Thus, at T_{c} or just below T_{c}, one can expand Δ up to first order. That is, one linearizes the self-consistent equation, Eq. (2.15).

Let $\hat{S} = \sum_{s\bar{s}} \hat{S}^{\bar{s}}_{s}$, where $s$and$\bar{s}$ respectively label the orbitals and bands, be the unitary matrix that diagonalizes $\hat{H}_0(k)$ and $\xi_{\bar{s}}(k)$ the energy bands of the normal state, one then obtains the linearized gap equation as, (see appendix A for details)

$$\Delta^{\eta}_{sr,a} = \sum_{ijb} \hat{M}^{\eta}_{sra;ijb}\Delta^{\eta}_{ji,b} \tag{2.18}$$

where the *stability matrix* $\hat{M}$ is given by,

$$\begin{aligned}\hat{M}^{\eta}_{sra;ijb} = &-\frac{\Gamma^{\eta}_{sr}}{4}\sum_{k\alpha\beta\bar{r}\bar{s}}\left[\left[\bar{\sigma}^{\eta}\right]_{\beta\alpha}\hat{S}^{\bar{s}}_{s}(k)\,\hat{S}^{\bar{r}*}_{r}(k)\,e^{ik\cdot a} - \left[\bar{\sigma}^{\eta}\right]_{\alpha\beta}\hat{S}^{\bar{r}*}_{s}(k)\,\hat{S}^{\bar{r}}_{s}(k)\,e^{-ik\cdot a}\right] \\ &\times\left[\left[\bar{\sigma}^{\eta}\right]_{\alpha\beta}\hat{S}^{\bar{r}}_{i}(k)\,\hat{S}^{\bar{s}*}_{j}(k)\,e^{-ik\cdot b} - \left[\bar{\sigma}^{\eta}\right]_{\beta\alpha}\hat{S}^{\bar{s}*}_{i}(k)\,\hat{S}^{\bar{r}}_{j}(k)\,e^{ik\cdot b}\right]\chi^{\bar{r}\bar{s}}(k)\end{aligned}$$

with

$$\chi^{\bar{r}\bar{s}}(k) = \left[\frac{\tanh\left(\frac{\beta\xi_{\bar{r}}(k)}{2}\right) + \tanh\left(\frac{\beta\xi_{\bar{s}}(-k)}{2}\right)}{\xi_{\bar{r}}(k) + \xi_{\bar{s}}(-k)}\right].$$

the *pair susceptibility* which gives the information on the propensity of a system to exhibit superconductivity, where $\beta = 1/k_{\mathrm{B}}T$ with T the temperature and k_{B} the Boltzmann constant.

The right hand side of Eq. (2.18) is the response of the order parameters, the vector $\Delta^{\eta}_{sr,a}$, to perturbations. The stability matrix is a response matrix whose eigenvalues determine if an order given by the corresponding eigenvector is an instability of the system. At T_c the vectors Δ of the order parameters on both sides of Eq. (2.18) are equal if Δ is a superconducting state of this system. Hence, $\Delta^{\eta}_{ji,b}$, can be interpreted as an eigenvector of the stability matrix with unity eigenvalue. Thus, at T_{c} any eigenvector of $\hat{M}$ with unity eigenvalue is superconducting, and symmetry of its corresponding eigenvector gives the symmetry of the superconducting order parameter, $\Delta^{\eta}_{ji,a}$, (eigenvectors with eigenvalues greater than unity are already below T_{c}). Thus, by tuning T until an eigenvalue of unity is obtained one can predict the T_{c} of a superconductor. The symmetry of the order parameter, will be expatiated in the next chapter.

2.3.1 Conventional and unconventional superconductors

Earlier in section 2.2.1, the explanation of the mechanism through which a material becomes superconducting was shelved. The exposition of the features of a superconductor given in preceding discussions is enough for the understanding of the mechanism of superconductivity. It is time to discuss the origin of the interaction that leads to superconductivity.

Consider a material with simple atomic arrangement in the lattice such that the normal state has only one band. Assume that parity is conserved,[3] then, $\hat{S} = 1, \bar{s}, \bar{r} = 1, \xi(k) = \xi(-k)$ in Eq. (2.18). Then the gap equation for this fictitious material for different interaction range can be local or nonlocal in space.

On-site superconductivity

For onsite superconductivity the interaction is localized to a site, that is $a = b = 0$. Due to Pauli exclusion principle the spin part of the order parameter must be singlet, $\bar{\sigma}^{\eta} = \bar{\sigma}^{0}$. Then the linearized gap equation, Eq. (2.18), reduces to

$$\Delta^{0}_{rr} = -\Gamma^{0}_{rr} \sum_{ik} \frac{\tanh\left[\frac{1}{2}\beta\xi(k)\right]}{2\xi(k)} \Delta^{0}_{ii}, \tag{2.19}$$

where the order parameter, Δ^{0}_{rr}, is constant in k. This superconducting state is called *on-site s*-wave superconductivity, denoted by s_{on} for the remainder of this Thesis. Taking $i = r = 0$ one obtains the archetypal textbook gap equation. On-site superconductivity is ubiquitous in elemental superconducting

[3] All materials studied in thesis are parity conserving in the normal state i.e. $\hat{H}_0(k) = \hat{H}_0(-k)$.

materials. This is the superconducting state described by the original BCS Hamiltonian.

Since the order parameter for s_{on} is constant then $\Gamma^0_{r,r}$ must be attractive for the gap equation, Eq. (2.19), to have a solution. The bare interaction between paired electrons is repulsive on-site Coulomb interaction. Then, how can $\Gamma^0_{r,r}$ be attractive? For superconductivity this attractive interaction is an effective interaction resulting from the combination of Coulomb and electron-phonon interactions. It was first shown by Frölich [55] and then by Barbeen and Pines [56] that attractive electron-phonon interaction can overcome the repulsive Coulomb interaction leading to an effective attractive interaction. This effective attractive interaction was preconceived when proposing the BCS theory. The attractive interaction comes from shielding of electron by phonons as the electron moves around in the lattice, leading to an effective positive charge, which then attracts another electron. The short story is that the attraction between the electrons is phonon-mediated.

In this Thesis, for $s-$wave superconductivity Γ (referred to as V_{sc} in the Papers of this Thesis) is taken to be attractive and the actual mechanism of the phonon exchange is ignored. This is called *weak-coupling* theory. The *strong-coupling* or Eliashberg theory incorporates the mechanism of phonon mediation through retardation but this is not of interest in this Thesis.

Nonlocal and higher momentum superconductivity

When the paired sites are different,i.e. $a \neq 0, b \neq 0$, the order parameter is momentum dependent. Hence, the interaction is nonlocal in space. Here, the spin part can be singlet or triplet. The gap equation, Eq. (2.18), then becomes

$$\Delta^{\eta}_{sr,a} = -\Gamma^{\eta}_{s,r} \sum_{ijkb} g^{\eta}(k) \frac{\tanh\left[\frac{1}{2}\beta\xi(k)\right]}{2\xi(k)} \Delta^{\eta}_{ji,b}, \tag{2.20}$$

where the nature of the function $g^{\eta}(k)$ depends on the spin configuration, η. Unlike the on-site superconductivity the nonlocal superconductivity is momentum dependent.

There are two scenarios for the solution of the gap equation, Eq. (2.20). In the first case the interaction is attractive, due to electron-phonon interaction, but then the gap, more specifically the right hand side of Eq. (2.20), has to be isotropic in momentum space. Such superconducting state is termed extended s-wave, s_{ext}, because it has the same symmetry as $\xi(k)$. The reason for this terminology will become clear when symmetry is discussed in section 2.5 below. The second possibility is when the interaction is repulsive. This is when pure electronic interaction leads to superconductivity. For this to be possible the order parameter must change sign in momentum space for the gap equation to have a solution. Thus, a higher order momentum dependent gap is formed by developing nodes in order to satisfy the gap equation. These superconducting states are termed d-, g-wave (p-, f-wave) for spin-singlet (spin-triplet) super-

conductivity. Superconductors with s_{on} or s_{ext} are said to be conventional. Most metallic superconductors, e.g. Pb, and Nb, are conventional with s_{on} superconductivity. Some iron-based superconductors are believed to have s_{ext} gap.

Superconductors with gaps with nontrivial momentum dependence are called unconventional superconductors. For example cuprate superconductors are unconventional superconductors with $d-$wave superconducting gap.

Determination of the symmetry of the superconducting gap will be discussed in the next chapter but before that let us shift gear from intrinsic superconductivity to *induced* superconductivity.

2.4 Proximity effect

The discussion in the preceding sections are based on intrinsic superconductivity. In the case of intrinsic superconductivity the gap equation has solutions. However, there exist many materials that do not condense into a superconducting state. Placing such materials next to a superconductor can still make the nonsuperconducting material amenable towards superconducting correlations [68]. This effect called *proximity effect* occurs through Andreev reflection where Cooper pairs leak into the (previously nonsuperconducting) material [62] making it superconducting. Proximity effect has become a standard method for creating unconventional and *topological* superconductors. Proximity effect dominates application of superconductivity in technology and the research in this field is very active.

To understand this effect consider a nonsuperconducting material with Hamiltonian $\hat{H}_0^{\text{n}}$ in proximity to a superconductor with Hamiltonian $\hat{H}_0^{\text{sc}}$. The coupling between the two materials is $\hat{\Gamma}$. The total Hamiltonian is

$$\hat{H} = \begin{pmatrix} \hat{H}_0^{\text{n}} & \hat{\Gamma} \\ \hat{\Gamma}^{\dagger} & \hat{H}_0^{\text{sc}}. \end{pmatrix} \tag{2.21}$$

The total Green function $G(\omega) = \left(i\omega - \hat{H}\right)^{-1}$ can be written as

$$\hat{G} = \begin{pmatrix} \hat{H}^{\text{n}} & \hat{\hat{\Gamma}} \\ \hat{\hat{\Gamma}}^{\dagger} & \hat{H}^{\text{sc}} \end{pmatrix}^{-1} \tag{2.22}$$

where $\hat{H}^{\text{i}}$ is the effective Hamiltonian of material i after proximity effect and $\hat{\hat{\Gamma}}$ the new coupling. After some algebra one gets

$$H^{\text{n}} = H_0^{\text{n}} + \hat{\Gamma}\,(i\omega - H_0^{\text{sc}})^{-1}\,\hat{\Gamma}^{\dagger} = H_0^{\text{n}} + \Sigma\big(\omega\big) \tag{2.23}$$

The effective Hamiltonian of the nonsuperconducting material after being proximitized to the superconductor, H^{n}, has superconducting correlations which

enter through the self-energy, Σ. However, the type of superconductivity that develops in the material is influenced by the superconducting state of the original superconductor and also by the nature of the nonsuperconducting material [69]. As seen from Eq. (2.23) the off-diagonal part of $\hat{G}_0^{\mathrm{n}}$, which contains the induced superconducting correlations, depends on both $\hat{G}_0^{\mathrm{n}}$ and $\hat{G}_0^{\mathrm{sc}}$.

In this Thesis graphene in proximity to an unconventional superconductor [23] and nanowire in proximity to a conventional superconductor [39] are studied.

2.4.1 Effective one-dimensional superconductor

Due to large quantum fluctuations superconductivity does not occur in 1D. However, effective 1D superconductors have been engineered in the laboratory through proximity effect. The last fifteen years have seen enormous effort on effective 1D superconductors with spin-orbit coupling and Zeeman interaction. This comes as a result of the proposal that such system host Majorana bound states and therefore could be used for topological quantum computation. Several methods have been used to realize effective 1D superconductor. The two most prominent approaches being (1) semiconducting nanowire with strong spin-orbit coupling proximitized to *s*-wave superconductor [32], and (2) magnetic impurity chain deposited on a spin-orbit coupled superconductor [33]. Ignoring magnetism for now, and focusing on the superconducting nanowire, the effective 1D Hamiltonian is[4]

$$\begin{aligned} H_0^{\mathrm{n}} = &\sum_{k_x\alpha\beta} d^\dagger_{k_x\alpha}\big[-2t_n\cos\left(k_x\right)\sigma^0_{\alpha\beta} - 2i\alpha_{\mathrm{soc}}\sin\left(k_x\right)\sigma^y_{\alpha\beta}\big]d_{k_x\beta} \\ &+\Delta_0\sum_{k_x} d^\dagger_{k_x,\uparrow}d^\dagger_{-k_x\downarrow} + \mathrm{H.c.} \end{aligned} \tag{2.24}$$

where the operator $d_{k_x\beta}$ destroys an electron with spin β and momentum k_x in the NW, α_{soc} is the strength of Rashba spin-orbit coupling along y-direction, t_{n} is the hopping strength in the NW, Δ_0 is the induced superconducting gap.

Figure 2.1 shows the energy bands of the effective 1D superconductor described by Eq. 2.24. Panels (a,c) show the electron (gold) and hole (blue) bands in the nonsuperconducting state. The bands are degenerate in Panel (a) when there is spin-orbit coupling but the degeneracy is lifted in Panel (c) in the presence of spin-orbit coupling. Panels (b,d), for the superconducting phase,

[4]Note that it is assumed that the superconductor is large. For proximitized nanowire in the weak coupling regime the main effect of the superconductor is inducing superconducting correlation in the nanowire [70]. In this case the semiconducting nanowire becomes a superconductor and can be studied independently. It is worth mentioning in the strong coupling regime one cannot treat the nanwire and superconductor separately because the superconductor renormalizes all the NW parameters. In this case the full NW+SC system has to be treated as a single entity [71, 39]. The strong coupling limit case will be discussed in section 5.3

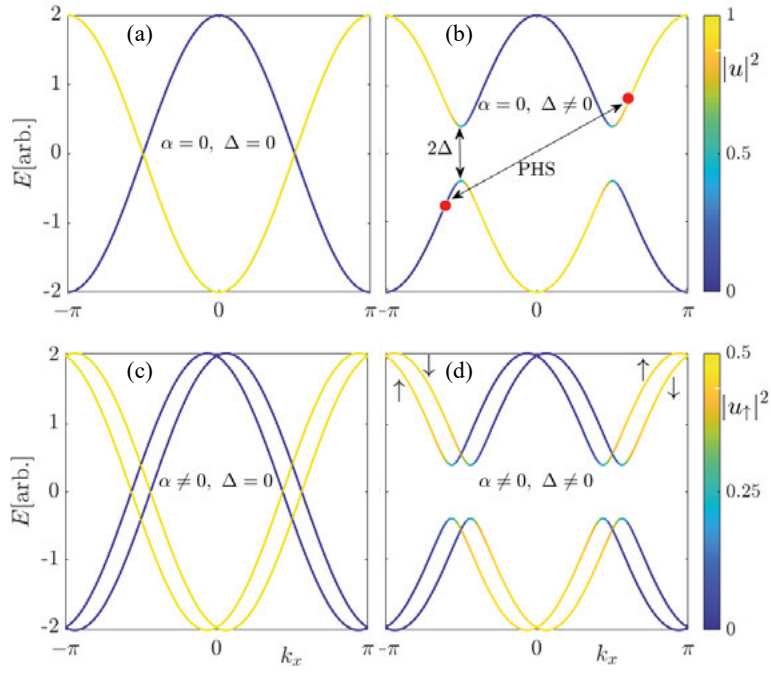

Figure 2.1. Energy of s-wave superconductor as a function of k_x showing the normal state without spin-orbit coupling (a) and its corresponding superconducting state (b), normal state with spin-orbit coupling (c) and its corresponding superconducting state (d). Spin-orbit coupling lifts the degeneracy in the bands except at $k_x = 0, \pi$, which reflects the so-called Kramer's degeneracy. The electronic amplitude, $|u|^2$, has been mapped on the energies such that gold (blue) denote electrons (holes), see color bar. Note that the color around $E = \pm\Delta$ in (b,d) shows a mixture of electrons and holes. When $\Delta = 0$, the normal state (a) contains pure electrons (yellow) and pure holes (blue). Turning on superconductivity, (b), hybridizes the electrons and holes around Fermi energy, $E_F = 0$ in this case, opening a gap of 2Δ. For $\alpha \neq 0$, the normal state bands are shifted along k_x and the degeneracy between spin-up and spin-down states is lifted but the bands are mixed (c). Turning on superconductivity gaps out all degeneracies around E_F but the Kramer's degeneracies, protected by time reversal symmetry, remain (d). Note how PHS relates the states (representative points in red dot) to each another.

show that superconductivity mixes electrons and holes around the Fermi energy and thereby creates an energy gap of $2\Delta_0$ symmetrically around zero energy. The high energy degeneracies at $k_x = 0, \pm\pi$ for finite spin-orbit coupling, see Figure 2.1(c,d), are the Kramer's pairs. The Kramer's pair degeneracy can only be lifted by breaking time-reversal symmetry.

There is more to this simple superconductor: by applying sufficient magnetic field it becomes a topological superconductor. Features of this 1D superconductor has been a subject of intense study for the past ten years and is

still very active. At this point it is necessary to discuss notion of topological superconductivity before applying magnetic field. This will done in Chapter 3.

2.5 Symmetry aspects of superconductivity

Superconducting materials usually have an underlying crystal structure. The arrangement of atoms in the lattice of a crystal influences the electronic behavior of the system. A lattice has unique symmetries with reference to a point in the lattice. The presence of symmetries not only reduces the complexity of a problem but also gives insight into the nature of the system, and one can obtain valuable information about the system without doing much calculations. For example, as we have seen before, PHS constrains the eigenvalues of the BdG Hamiltonian to come in pairs but with opposite signs. Interestingly, the symmetry operations of a lattice form a group. Thus, each lattice can be classified according to a specific point group. A point group contains all the symmetry operations except translation.[5] A key property of groups is that each group element can be represented by a matrix. This is the concept of representation theory and this field is called group theory. In the following, relevant lattice geometries and superconducting states that are of interest to this Thesis are briefly discussed, within group theory. Details of group theory can readily be found in textbooks [72, 73], while character tables can be found well-documented online [74, 75], as well as visualization of symmetry operations [76].

2.5.1 Definition of key group theoretical concepts

Conjugacy and Class: Let g_i be the elements of the group $\mathcal{G}$. Element g_1 is conjugate to g_2 if $g_2 = g_3 g_1 g_3^{-1},\ \forall\ g_1,\ g_2,\ g_3 \in\ \mathcal{G}$. Conjugacy is an equivalence relation, implying that conjugate elements have some common properties, hence they can be categorized. The collection of all elements that are conjugate to each other is called a *class*. An example of conjugacy is Eq. (2.17). This suggests that both $\hat{H}_{\mathrm{BdG}}$ and $-\hat{H}^T_{\mathrm{BdG}}(-k)$, discussed in section 2.2.4, belong to the same class and are related through PHS. Furthermore, $\hat{H}_{\mathrm{BdG}},\ -\hat{H}^T_{\mathrm{BdG}}(-k)$, and $\mathcal{P}$ are all elements of the same group.

Representation: A representation Γ of a group $\mathcal{G}$, with group multiplication $\circ$, is a group of nonsingular square matrices $\hat{M}$ such that the matrices satisfy the properties of a group: If $g_1 \circ g_2 = g_3,\ \forall\ g_1, g_2, g_3 \in \mathcal{G}$ then $M(g_1)M(g_2) = M(g_1 \circ g_2) = M(g_3) \in \Gamma$, where $M(g)$ is the matrix representing element $g \in \mathcal{G}$.

Reducible and irreducible representations: A representation is called a *reducible representation* if it is decomposable to a direct sum of other rep-

[5] By including translations one obtains a space group.

D_{6h}	E	$2C_6$	$2C_3$	C_2	$2C_2'$	$2C_2''$	i	$2S_3$	$2S_6$	$3\sigma_h$	$3\sigma_d$	$3\sigma_v$	Basis function
A_{1g}	+1	+1	+1	+1	+1	+1	+1	+1	+1	+1	+1	+1	$1,\ k_x^2+k_y^2$
E_{2g}	+2	-1	-1	+2	0	0	2	-1	-1	+2	0	0	$k_x^2-k_y^2,\ k_xk_y$
B_{1u}	+1	-1	-1	-1	-1	+1	-1	-1	+1	-1	+1	-1	$k_x(k_x^2-3k_y^2)$
E_{1u}	+2	+1	-1	-2	+1	+1	-2	-1	+1	+2	-1	-1	$k_x,\ k_y$

Table 2.1. *Character table showing relevant irreducible representations (first column) of the honeycomb lattice in D_{6h} point group. The entries in the first column are the irreducible representations relevant to this Thesis. The full D_{6h} point group character Table has twelve irreducible representations. The top row (columns 2-13), contains the classes in the form N_kC_k, where N_k is the number of elements in the class and C_k is the representative symmetry operation of the class. The entries under the classes for each irreducible representationare the characters, χ of the irreducible representations under the symmetry operations C_k. The character of an irreducible representation under the identity element, E, gives the degeneracy of the irreducible representation. The last column contains the basis functions, which gives the spatial behavior of the irreducible representations. Here, a 2D lattice is considered, such that $k_z = 0$, and the representative basis function up to cubic order. The top (bottom) half is even (odd) under inversion. See Ref.[73] for naming of point groups, symmetry operations, and labeling of irreducible representations. Some of the symmetry operations are shown in figure 2.2. See appendix B for the derivation of superconducting state.*

resentation. A reducible representation introduces ambiguity since any two representations can be combined to form a new one.

Any representation that cannot be reduced into a direct sum of other representations is called an *irreducible representation*. The irreducible representations of a symmetry group are orthogonal. In group theory, to remove ambiguity in the representations, only irreducible representations of the symmetry group are considered.

Character of a representation: The representation matrix $\hat{M}^{(\Gamma)}$ is arbitrary because the matrix $\hat{M}'^{(\Gamma)} = \hat{U}\hat{M}^{(\Gamma)}\hat{U}^{-1}$, where $\hat{U}$ is an invertible matrix, obtained by similarity transformation is also a representation of Γ. However, traces are unchanged under similarity transformation so $\hat{M}$ and $\hat{M}'$ have the same trace. In group theory the important quantity is the trace, called character χ. Elements in the same class are related by similarity transformation (conjugacy) implying that the representation matrices of elements in the same class have the same character. For example, it is trivial to deduce that $\hat{H}_{\mathrm{BdG}}(k)$ and $-\hat{H}^T_{\mathrm{BdG}}(-k)$ have the same character since the diagonal of a matrix is not affected by transpose operation.

Character table: The irreducible representations of a point group along with the classes of the symmetry operations and their characters are listed in a character table. The character tables of all known point groups have been calculated [72, 73, 74, 75].

Chapter 6 of this Thesis is devoted to the honeycomb lattice, specifically, graphene. The point group of the honeycomb lattice is D_{6h}. The character

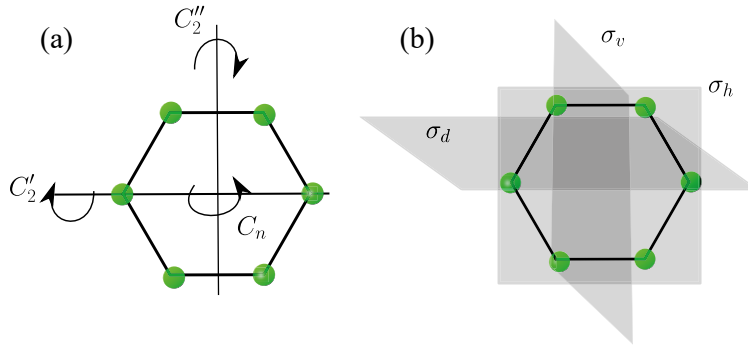

Figure 2.2. The symmetry operations of the honeycomb lattice belonging to the D_{6h} point group for rotations (a) and reflections (b). The C_n represent rotations by $\frac{2\pi}{n}$ through the principal axis while σ's are reflection planes. See Ref. [73] for definition of symmetry operations. Note only one of the three σ_d, σ_v, C_2' and C_2'' is shown. The improper rotations S_n are not shown but can easily be generated from $C_n\sigma_\mathrm{h}$.

table of the D_{6h} point group for $k_z = 0$, showing only irreducible representations relevant to this Thesis, is presented Table 2.1. The symmetry operations of the unit cells of the honeycomb, one for each class, are shown in Fig. 2.2. See Ref. [73] for complete definition of symmetry operations and irreducible representation labeling. The first column in the tables are the irreducible representations while the other columns (except the last one) are the classes and the number entries are the characters of the symmetry operations in each irreducible representation. The character of an irreducible representation under the identity class E gives the dimension of the irreducible representation. So $E_{2g}\left(A_{1g}\right)$ is a two (one) dimensional irreducible representation. The trivial representation A_{1g} have the full symmetry of the lattice while all other irreducible representations break some spatial symmetry.

Basis functions of irreducible representations: At times it is difficult to write down the representation matrices $\hat{M}$ of the symmetry operations of an irreducible representation. In this case it may be easier to know how the irreducible representation behaves in coordinate space. Basis functions gives information on the spatial behavior of an irreducible representation. Basis functions are often listed together with the characters in the character table. In the last columns of Tables 2.1 basis functions in reciprocal space, up to cubic order, of relevant irreducible representations are listed.

Projection operator: In mathematics the projection operator maps an object onto another object. In group theory, the projection operator is a special and very powerful tool in determining basis functions. Here, the projection operator $\hat{\mathcal{P}}_k^{\Gamma_n}$, for an irreducible representation Γ_n, maps a basis function of Γ_n on itself. If $\hat{P}_R$ is the symmetry operator of symmetry operation (i.e. group

element) R, then the projection operator is defined as [72, 73]

$$\hat{\mathcal{P}}^{\Gamma_n} = \frac{\dim[\Gamma_n]}{[g]} \sum_k N_k [\chi^{\Gamma_n}(C_k)]^* \hat{P}_R. \tag{2.25}$$

where $\dim[\Gamma_n]$ is the dimension of the irreducible representation (given by the character of symmetry element E), $[g]$ is number of group elements, N_k is number of elements in class $N_k C_k$, $\chi^{\Gamma_n}(C_k)$ is the character of symmetry operation C_k under the irreducible representation Γ_n see Table 2.1.

The projection operator simplifies the process of finding the basis function in that one only needs to know the characters of the symmetry operation under the irreducible representation of interest. Then, one finds how the function transforms according to the irreducible representation. Let $f^{\Gamma_n}(r)$ be a basis function of the irreducible representation Γ_n, then it satisfies

$$\hat{\mathcal{P}}^{\Gamma_n} f^{\Gamma_n}(r) = f^{\Gamma_n}(r) \tag{2.26}$$

One problem is that this approach of finding the basis function seems to be a *trial and error* method. It may become laborious and tiresome to find the right basis function. Group theory solves this ambiguity in the way basis functions are chosen. The basis functions are chosen from the harmonics expansion of the problem. For example, for isotropic, square, and honeycomb lattice systems one uses, respectively, spherical, cubic and hexagonal harmonics expansion as basis functions.For superconductivity, and in this Thesis, the basis functions are obtained using the eigenvectors of the linearized gap equation, Eq. (2.18), by expanding its corresponding momentum dependent factor around high symmetry points of the first Brillouin zone (1BZ). Further discussion is presented in section 2.5.3 below and application to honeycomb lattice is presented in chapter 6.

For the D_{6h} point group, representing the symmetry of graphene, there are twelve classes and irreducible representations, from the twenty-four group elements. Thus, calculating the projection operation on some arbitrary basis function can be algebraically complicated. This complication can be avoided through symbolic computation. A demonstration of the power of the projection operator is given in Appendix C, using Mathematica.

All group theoretical concepts important to the subject of this Thesis has been discussed. Attention will now be shifted on how this is connected to condensed matter physics and more importantly superconductivity.

2.5.2 Normal state

The normal state, described by the noninteracting Hamiltonian, is invariant under all the symmetry operations of the full group $\mathcal{G}$ satisfied by the interacting Hamiltonians in Eqs.(2.1), (2.4), (2.14). The full group $\mathcal{G} = G \otimes \mathcal{T} \otimes \mathrm{SU}(2) \otimes \mathrm{U}(1)$, where G is the point group of the crystal lattice, $\mathcal{T}$ represents

time-reversal symmetry (TRS) group, SU(2) the spin rotation group (important for spin-orbit coupling) and U(1) the gauge symmetry group. Note that if the spin-orbit coupling is strong, SU(2) and G cannot be treated independently but rather combined together and treated as a single group. This is the case for e.g. heavy fermion superconductors [59]. Here spin-orbit coupling and spatial symmetry are considered separately because graphene has negligible spin-orbit coupling. In fact, only spatial symmetry is of interest, $\mathcal{T}$ and SU(2) are postponed to the next chapter where topological superconductivity is discussed. The normal state does not break any symmetry in G. Thus, normal state always to the irreducible representation with highest symmetry in G. For example, in D_{6h} for honeycomb lattice, the normal state belongs to the perfectly symmetric A_{1g} irreducible representation, see Table 2.1.

2.5.3 Superconducting state

It is time to make connection with superconductivity. First, as discussed in section 2.2.2, superconductivity spontaneously breaks the U(1) gauge symmetry through its pair amplitude, $F \propto \langle cc \rangle$. If a superconducting state breaks another symmetry in addition to $U(1)$ it is referred to as unconventional but otherwise conventional.

The quest is to know which symmetry operations of $\mathcal{G} \setminus U(1) = G \otimes \mathcal{T} \otimes$ SU(2) are broken by the superconducting state, more specifically the order parameter, and then find the largest subgroup $H \subseteq \mathcal{G} \setminus U(1)$ where the order parameter is invariant. Here the focus is on the lattice spatial symmetry. Hence, it is necessary to find the largest subgroup $H \subseteq G$ under which the order parameter is invariant.

Although the lattice allows for several possible states, order parameters belonging to different irreducible representations usually have different T_c [77, 78, 11, 20]. As seen in Eq. (2.18) the linearized gap equation is an eigenvalue equation and its solutions belong to specific irreducible representations of the normal state. The highest eigenvalue determines the symmetry of the order parameter at T_c [77]. If the solution of the linearized gap equation has a degeneracy, all the degenerate solutions have the same T_c and belong to the same irreducible representation. Examples of this are the two-fold degenerate d-wave states on the honeycomb lattice, belonging to the two-dimensional E_{2g} irreducible representation, see Table 2.1. See appendix B for the derivation of superconducting states of graphene.

It is common for lattices to have several irreducible representations in a point group, as already seen in Table 2.1, where only the irreducible representations common for the solution of the gap equation, i.e the superconducting symmetries in graphene systems are listed. Note that apart from the s-wave states, the other superconducting states break some of the symmetries of the point group G and are therefore unconventional. The superconducting state

is named based on the spatial behavior of the basis function. When the basis function of the trivial representation is constant it is called s-wave, but when it has spatial dependence, which is isotropic, it is called extended s-wave. Both belong to A_{1g} irreducible representation, see Table 2.1. In this case $H = G$. The spatial symmetry breaking states under E_{2g} and B_{1u} are respectively d-waves and f-wave superconducting states.

Close to T_c the superconducting state can be a linear combination of several basis functions of the irreducible representation with the largest eigenvalue. Below T_c, as the temperature reduces further usually a few linear combinations can satisfy the nonlinear gap equation. Degenerate states belonging to the same irreducible representations can mix to form a more energetically favorable state. Indeed, on the honeycomb lattice, it has been shown that an equal complex mixture of the nodal d-waves, in E_{2g} irreducible representation, forming the fully gapped chiral $d_{x^2-y^2} \pm id_{xy}$-wave superconducting state, is the most stable state at doping close to the van Hove singularity [11, 20, 12, 13]. Note that the chiral states are topological with nonzero winding numbers.

Since the irreducible representations are orthogonal they should not mix. But this does not mean the superconducting state is always pure far below T_c. If there is a breakdown of continuous or structural symmetries as temperature decreases, then the eigenvector of the largest eigenvalue will no longer be an eigenstate of the eigenvalue equation [77]. In this case there can be a mixture of superconducting states, where a sub-dominant superconducting state mixes with the dominant one. A common form of this state is $d + is$ proposed to exist in cuprates [79], and recently $d + ig$ in Sr_2RuO_4 [80, 81].[6] Superconducting states with sub-dominant orders are not subject of interest in this Thesis.

As discussed earlier one can achieve superconductivity in an otherwise non-superconducting material through proximity effect. In Ref. [18] a cuprate superconductor is proximitized with graphene in an scanning tunneling spectroscopy experiment and the results showed induced superconductivity in the graphene layer. As shown in section 2.4, both d-wave superconductivity in the cuprate and the graphene lattice symmetry determine the induced superconducting state in graphene but only spin-singlet superconductivity is allowed since there is no spin-flipping terms in graphene. In Paper IV, various possible superconducting state on graphene proximitized with a cuprate superconductor are probed using a single potential impurity. The impurity quasi-particle

[6] Initially, Sr_2RuO_4 was proposed to be a candidate material for chiral $p_x \pm ip_y$-wave superconducting state [82, 83, 84, 85]. However, recent nuclear magnetic resonance experiment [86] has challenged this existence of chiral p-wave superconducting state in Sr_2RuO_4. Over the last two years, and currently, there is a continuous paradigm shift on the superconductivity of this enigmatic material. Though the superconductivity continues to mystify experts, after more than 25 years of efforts, there has been several new theoretical predictions of the superconducting state, e.g. see Ref. [80, 81]. It is now considered to be a spin-singlet even-parity superconductor. Understanding superconductivity of this material is important because it will shed light understanding superconductivity in its counterpart, the strongly correlated cuprate superconductors.

interference reveals the symmetry of the superconducting state in the lattice. Using this approach the superconducting state can be predicted in scanning tunneling spectroscopy experiments [87, 88, 89, 90].

3. Topological superconductors

In section 2.5, the classification of superconductivity was based on the symmetries of the order parameter, which are discrete symmetries of the lattice. Additional classification of superconductor based on quantum symmetries exists. This classification is topological and the exotic superconductors in this classification are called topological superconductors [29, 91, 92, 93, 94], a name that comes from the field of topology in mathematics. These superconductors have been a subject of intense study since their discovery [95, 24]. The most prominent feature of topological superconductors is the existence of robust gapless boundary states, despite the bulk being gapped. These boundary states can be localized or propagating depending on the topology of the superconductor. The subject of this chapter are the topological superconductors.

In mathematics, topology is a concept of classifying objects according to their shapes [96]. Two objects that can be continuously deformed into each other are said to be topologically equivalent and otherwise topologically inequivalent. A condensed matter system can be nontopological (same as trivial topology) or topological (same as nontrivial topology). The latter is the interesting case. By tuning parameters of a system it is possible to drive the system from nontopological phase to a topological phase. The system can also be driven between between two distinct topological phases. When this happens the system is said to undergo a topological transition. However, unlike usual phase transition between disordered and ordered phases, a topological phase transition between distinct topological phases involves coming across a topological defect which obstructs smooth deformation between these phases. In real systems this is related to closing and reopening of the gap energy. In other words when a system undergoes a topological phase transition its gap closes and reopens. A topological phase has a topological invariant which does not change during deformation except the gap closes, that is when there is an obstruction in the deformation, such that the topology of the system changes. Thus, topological invariants can be used to classify topological phases.

The topology of noninteracting Hermitian condensed matter systems and their topological invariants have been studied in detail. All such systems are classified into ten topological classes in the so called tenfold-way scheme [95, 24, 97]. The classification is based on the presence or absence of any or all of three quantum mechanical symmetries in the system, namely: particle-hole symmetry (PHS), time reversal-symmetry (TRS) and chiral symmetry. The chiral symmetry is proportional to the product of TRS and PHS, implying that if any two of the symmetries are present, then the third must be present.

Class	Symmetries				Dimension		SC	Edge states	Materials
	$\mathcal{T}$	$\mathcal{P}$	$\mathcal{C}$	SU(2)	1	2			
D	–	✓	–	–	Z_2	Z	spinless p-wave	MBS	Δ_s+SOC+B
C	–	✓	–	✓	–	$2Z$	chiral $d+id$	chiral electrons	graphene

Table 3.1. *Table showing classification of TRS breaking topological superconductors, class C and D (first column). The entries under Dimension are the topological invariants (bold entries are those relevant to this Thesis). The last three columns are, respectively, nature of superconducting state, type of edge states, and the material where these topological superconductors can be physically realized. Here MBS implies Majorana bound state, SOC implies spin-orbit coupling and Δ_s+SOC+B indicates combination of different materials namely: s-wave superconductor, Rashba SOC material, and application of external magnetic field, to engineer the superconductor.*

As seen in section 2.2.3, the BdG formalism of superconductor has built-in PHS. Focusing on TRS breaking superconductors, then chiral symmetry must vanish, which means only PHS exists. Superconductors which break TRS can exhibit topology in the tenfold-way scheme depending on spin rotation. The superconductor can be class D with broken spin rotation symmetry or class C with preserved spin rotation, see Table 3.1. Details of the classification of topological superconductors can be found in the literature [93, 98].

This Thesis studies 1D Class D topological superconductors engineered in real materials, and 2D Class C topological superconductors in graphene, under different types of defects.

3.1 Topological invariant in quantum mechanics

For a quantum mechanical system the topological invariant is encoded in the wave function and can be obtained from the Berry phase [99]. If $|\psi^\nu(k)\rangle$ is an eigenstate of $\hat{H}_{\text{BdG}}$ with eigenvalue $E^\nu(k)$ where ν labels the bands, then the Berry phase, θ, along a curve C is given by [92, 93]

$$\theta_\nu(C) = \oint_C A^\nu \cdot dk, \quad A^\nu = i\langle\psi^\nu(k)|\nabla_k\psi^\nu(k)\rangle, \tag{3.1}$$

where A^ν is the Berry potential, which is gauge dependent since the phase of $|\psi^\nu(k)\rangle$ is not fixed. Choosing a new gauge such that $|\psi'^\nu(k)\rangle = e^{i\phi_k}|\psi^n(k)\rangle$ one obtains the Berry phase in the new gauge as $\gamma'_\nu(C) = \theta_\nu(C) - \oint_C \partial_k\phi_k dk$. As long as C is a closed loop the integral in the second term is always a multiple of 2π. As such, the phase factor $Z = e^{i\theta'_\nu(C)} = e^{i\theta_\nu(C)}$ is an invariant. Note that $\theta_\nu(C)$ is path dependent.

The presence of PHS, as discussed in section 2.2.4, enforces that if $|\psi^\nu(k)\rangle$ is a state with energy $E^\nu(k) > 0$, then there is also a state $\mathcal{P}|\psi^\nu(k)\rangle = |\psi^{\nu*}(-k)\rangle$ with energy $E^\nu(-k) < 0$, (see figure 2.1(b) for visualization). In this case, summing over all occupied band contributions to Eq. (3.1), the total Berry

phase is quantized, $\theta = 2\pi m$, where m is an integer, see Ref. [93] for proof. The topological invariant is then $Z = \theta \mod 2\pi$. In this case, $Z = 0$ zero for trivial phase and $Z = 1$ for nontrivial topological phase.[1] Other values of topological invariant are possible depending on the symmetries of the superconductor, see Table 3.1.

Another topological invariant, called the Chern number, N, can be defined from the Berry connection as [100].

$$N = \frac{1}{4\pi} \int_{BZ} F \cdot dk, \quad \text{with } F = \nabla \times A, \tag{3.2}$$

where F is the Berry curvature, which is a gauge independent quantity.

This description of the topological invariant gives the misconception that it is some abstract object. However, in condensed matter physics the topological invariant is related to physical properties of the system which are conserved, and this quantity can be used as a topological invariant. Such physical property include quantized conductance [101, 102]. The number of edge states is also related to the topological invariant [27]. This relationship is given by the index theorem or bulk-edge correspondence. This theorem is briefly discussed below.

3.2 Bulk-edge correspondence

In the previous section, the concept of topological invariant was discussed in relation to bulk systems in momentum space. However, in experiments samples are usually small, and thus have edges. One can ask what is the meaning of a topological invariant or what are the features of topological states in these finite samples. The bulk-edge correspondence [27, 29, 28, 30] is a powerful theorem that gives physical meaning to the topological invariant. The theorem postulates that the boundary between two topologically different systems hosts zero energy states. This implies that the closure of the energy gap as the Hamiltonian is deformed from one topological class with topological invariant N_1 to another topological class with topological invariant N_2 is equivalent to the appearance of zero-energy states at the boundary between these two systems, provided that the boundary is between topologically distinct systems. The total number of edge states per edge is $|N_1 - N_2|$ [27]. Note that for vacuum the invariant is zero. Through the bulk-edge correspondence, the bulk topological invariant tells us exactly how many zero energy states will appear at the edge of finite system.

[1] The phase factor $Z = e^{i\theta}$ can also be chosen to be the topological invariant. Then, $Z = 1$ for topologically trivial phase and $Z = -1$ for topologically nontrivial phase.

3.3 Majorana fermions in condensed matter physics

In particle physics, Majorana fermions are particles that are their own antiparticles [61, 103, 104]. Being its own antiparticle, a Majorana fermion is necessarily neutral since particles and antiparticles have opposite charges. So the wave function is real. Neutrinos are candidates for Majorana fermions but there is no experimental evidence that confirms that neutrinos are their own antineutrinos, because neutrinos rarely couple with matter.

While Majorana fermions are still elusive in particle physics, there is now a strong evidence of their emergence as quasi-particles excitations in topological superconductors in condensed matter physics [103, 32, 105, 33]. To be a Majorana fermion an excitation must satisfy two criteria: (1) It must obey Dirac equation, and (2) be its own antiparticle. In topological superconductors there exist gapless states, according to the bulk-edge correspondence. Since the gapless state are linear around the Fermi energy then the low energy Hamiltonian will satisfy linear dispersion. Thus, the low energy states of topological superconductors obey the massless Dirac equation. Hence, the first criterion is fulfilled. The second criterion is fulfilled in a superconductor since the Bogoliubov excitations are linear combination of electrons and holes. Thus, the low energy excitations of topological superconductors are Majorana fermions, although they are not the same as their particle physics counterpart.

3.3.1 Majorana bound states

From Eq. (2.10) it is noted that the operator γ_ν is associated with positive energy excitations while the operator $\gamma_\nu^\dagger$ is associated with negative energy excitation, of a superconductor. Considering a zero energy state in a topological superconductor, i.e. $E^\nu = 0 = -E^\nu = E^0$, then from Eq. (2.10)

$$\gamma_0 = \gamma_0^\dagger = \gamma. \tag{3.3}$$

These zero energy states come in pairs due to PHS. In other words, if γ_1 exists at zero energy, then must be another γ_2 also at zero energy. These zero energy levels in a topological superconductor are called *Majorana zero modes* or *Majorana bound states*.[2] Here Majorana bound state is used. From Eq. (3.3) it is noted that γ both the creation and annihilation operator of the zero energy state. This is a contradiction. A way to resolve the problem is to consider two

[2] In real materials due to finite size effects, the Majoranas might not sit exactly at zero energy, although still very close to zero energy. In this case, which is often the case in reality, and even in numerically simulation, they are called Majorana bound states. Majorana zero mode is a special case of Majorana bound state when the Majoranas are exactly at zero. Here, Majorana bound states is used to refer to these Majoranas irrespective of their energy as long as the required properties are satisfied. In the literature there is no clear distinction between Majorana fermion Majorana bound state and Majorana zero mode.

Majorana operators, γ_1 and γ_2, and then define a complex fermion [91], as

$$c_m = \frac{1}{2}\left(\gamma_{m,1} + i\gamma_{m,2}\right), \qquad c_m^\dagger = \frac{1}{2}\left(\gamma_{m,1} - i\gamma_{m,2}\right), \tag{3.4}$$

where m labels the state, not site. In this way one can interpret a fermion as a combination of two Majorana zero modes and in reverse, the Majorana zero mode as half a fermion. Inverting the expression we obtain

$$\gamma_{m,1} = \left(c_m + c_m^\dagger\right) \quad \text{and} \quad \gamma_{m,2} = -i\left(c_m - c_m^\dagger\right). \tag{3.5}$$

It can be seen that $\gamma_{m,i}^\dagger = \gamma_{m,i}$ and the commutation relation $\{\gamma_m, \gamma_n\} = 2\delta_{mn}$. It should be noted that $\gamma_{m,1}$ and $\gamma_{m,2}$ can be separated in space. When the $\gamma_{m,1}$ and $\gamma_{m,2}$ are close, they combine so that c_m is a regular fermion, and no Majorana bound states in the system. However, when spatially separated $\gamma_{m,1}$ and $\gamma_{m,2}$ exist different points (boundaries according to bulk-edge correspondence), and the fermion c_m is a spatially nonlocal fermion. This nonlocal property has been shown to lead to the non-Abelian statistics of Majorana bound states [24], and also endows Majorana bound states with immunity against local perturbations. Also, the energy gap of the superconductor separates Majorana bound states from the continuum of states at higher energies. This is referred to as topological protection. These properties open the door for using Majorana bound states for fault tolerant quantum computation [40, 91, 106].

Majorana bound states have been proposed to exist at edges of 1D p-wave superconductors and at the center of vortices in chiral p-wave superconductors [24, 40, 91, 106]. Such superconductors belong to Class D topological superconductors, see Table 3.1. Single entity materials exhibiting these exotic superconducting phase are rare in nature. However, the superconductors can be engineered in the laboratory by combining several ingredients that satisfy the symmetries of Class D topological superconductors. The ingredients for achieving 1D p-wave superconductor is given in the last column of Table 3.1.

In summary, Majorana bound stateare topologically protected states which exists at the edges of 1D p-wave superconductors. In Paper I, the robustness and stability of Majorana bound states against perturbation was put to test by subjecting Majorana bound states at the end of a magnetic chain in a superconductor to strong disorder. The topological protection of Majorana bound states from finite energy quasi-particle poisoning improves with a large topological energy gap. One of the main issues in experimental realization of Majorana bound states in earlier experiments is that the topological gap was small [32, 105]. It has been shown that it is possible for zero-energy energy states on nontopological origin can appear in Majorana bound states experiments [36]. Distinguishing between this trivial zero-energy states and Majorana bound states has been a subject of debate [46, 45, 39, **?**, **?**, 48]. In Paper II, an approach for possible unambiguous detection of Majorana bound states through supercurrent is proposed.

4. Methods of solving the Bogoliubov-de-Gennes Hamiltonian

In chapters 2 and 3 superconductivity and its properties were discussed. What is missing is the methodology for obtaining necessary information about the superconducting state from $\hat{H}_{\mathrm{BdG}}$. This missing piece is filled in this chapter.

Due to the presence of defects, namely impurities, disorder, domain walls and junctions, in the materials studied in this Thesis, the studies are carried out in real space. This makes $\hat{H}_{\mathrm{BdG}}$ a large matrix . The size increases rapidly with lattice size. The problem is then a large eigenvalue problem. To solve this problem, one needs to consider the computational cost and the properties of the system to be studied. Two methods are used, namely diagonalization and spectral methods.

4.1 Diagonalization methods

Diagonalization of a Hermitian matrix is probably the most prominent topic in linear algebra. The method is very efficient since it gives access to the eigenvalues and eigenvectors with which one can calculate any observable. Numerically, depending on the size of the problem or target physics one can choose between full diagonalization and partial or Arnoldi iteration method of diagonalization.

4.1.1 Full diagonalization

This is the usual diagonalization method and will not be discussed here. After diagonalization one obtains eigenvalues E^{ν} and unitary matrix $\sum_{\alpha} U^{\nu}_{i\alpha}$, where denotes spin and i lattice sites. Any observable of interest can be calculated from the two quantities.

Numerically, the diagonalization method is very computationally expensive with computational time of order $\sim (4N)^3$ for $\hat{H}_{\mathrm{BdG}}$ with N lattice sites. The full diagonalization of $\hat{H}_{\mathrm{BdG}}$ in real space therefore limits study to smaller lattice sizes. The fact that one needs to tune parameters which entails diagonalizing the Hamiltonian several times implies that the size of the system needs to be small. While the size of the lattice may the small compared to experimental samples the method yields qualitatively accurate results when one uses large values of the superconducting order parameter. This is possible due to

the fact that the superconducting coherence length, ξ, is inversely proportional to the magnitude of the order parameter, $|\Delta|$, that is $\xi \propto |\Delta|^{-1}$. Realistically $|\Delta|$ is small, $\sim 1.0-3.0$meV for s-wave superconductors [33], albeit larger for unconventional superconductors. It is, therefore, necessary to ensure that the lattice is larger than ξ, for superconductivity to be stable, implying a large lattice. However, by using $|\Delta|$ values larger than experimental values ξ becomes small and one can simulate experimental scenarios with smaller lattice. Note that since $|\Delta|$ and ξ are numbers, thus this approach has no qualitative effect on the simulations.

Self-consistent calculation of the order parameter

Often in the literature, the superconducting state is studied using nonself-consistent analysis where the magnitude of the order parameter is assumed to be constant in space. However, as discussed earlier, the order parameter is locally affected by defects. Thus, when the superconductor is inhomogeneous the order parameter will vary with space. To capture its spatial behavior the order parameter is calculated self-consistently. In this Thesis, self-consistent calculations are carried out with the diagonalization method. This is because diagonalization gives access to the coherence factors u, v making it easy to calculate the order parameter directly from the self-consistent equation, described by Eq. (2.5), as

$$\begin{aligned}\Delta_{ji}^{\eta} &= \frac{\Gamma_{ij}}{2}\sum_{\alpha\beta\nu} U_{j\beta}^{\nu}\left[\overline{\sigma}_{\beta\alpha}^{\eta}\right]U_{i\alpha}^{\nu} f_{\mathrm{FD}}\left(\beta E^{\nu}\right) \\ &= -\frac{\Gamma_{ij}}{2}\sum_{\alpha\beta\nu}\left[\bar{\sigma}^{\eta}\right]_{\beta\alpha}\left[s_{\alpha}u_{j\beta}^{\nu}v_{i\alpha}^{\nu *} f_{\mathrm{FD}}\left(-\beta E^{\nu}\right)+s_{\beta}v_{j\beta}^{\nu *}u_{i\alpha}^{\nu} f_{\mathrm{FD}}\left(\beta E^{\nu}\right)\right],\end{aligned} \tag{4.1}$$

where f_{FD} is the Fermi function.

This method is used in Paper III where domain wall of chiral d-wave superconducting state was studied in semi-infinite graphene. To make the problem tractable to diagonalization the infinite direction was Fourier transformed to moment space while the finite direction is kept in real space. This significantly reduced the size of $\hat{H}_{\mathrm{BdG}}$. Thus, the self-consistent calculation is not expensive. The self-consistent calculations showed that the order parameter is suppressed at the domain wall making it possible to extract the domain wall width. In this mixed space, mixture of real x-axis and momentum space k_y in y direction, the *spectral function*, given by,

$$A\left(E,k_y,x\right)=\sum_{\nu=1}^{2N}\left(|u_{x,k_y}^{\nu}|^2+|v_{x,k_y}^{\nu}|^2\right)\left[\delta\left(E-E^{\nu}\left(k_y\right)\right)+\delta\left(E+E^{\nu}\left(-k_y\right)\right)\right] \tag{4.2}$$

tracks the flow of the states, especially the low energy states. Thus, it unambiguously discern between edge, domain wall and bulk states as well as indicate the flow direction in k-space.

Self-consistent calculation of the order parameter of a disorder superconductor was carried in Paper I. The self-consistent calculation in Paper I made it possible to obtain the condition for the stability of Majorana bound states at the end of magnetic chain in a spin-orbit coupled superconductor, which is not possible to find in nonself-consistent calculation.

It is worth mentioning that self-consistent calculation is computationally expensive since the diagonalization is carried out several times, until the order parameter converges. Therefore, self-consistent calculation could be avoided in situations where it does not have qualitative effect on the results. An example of situations where self-consistency may not be important is when a single potential impurity is deposited on a large superconductor.

4.1.2 Arnoldi iteration method

At times one may want to to study the system with experimentally realistic values. Often, the important features are the low energy states especially in the case of topological superconductors where zero-energy states are present at the defects as a consequence of bulk-edge correspondence. In such cases partial diagonalization using the Arnoldi iteration method [107, 108] is handy. The method use far less memory than required in a full diagonalization, thus drastically reduces the computational cost while simulating system size that is not feasible with full diagonalization method. The calculation can further be sped up if the Hamiltonian is a sparse matrix. The price of using this method is lack of information on some of the states. The Arnoldi method is one of the iterative methods used in obtaining the largest eigenvalues, in magnitude, of a matrix. When the target are the smallest eigenvalue the inverse of the matrix is used. In the case of this Thesis, the inverse of $\hat{H}_{\mathrm{BdG}}$ is used for to extract the smallest eigenvalues, since the inverse of the eigenvalues of the inverse of $\hat{H}_{\mathrm{BdG}}$ are the eigenvalues of $\hat{H}_{\mathrm{BdG}}$. This takes most of the computational time since inversion is an expensive operation. However, the Arnoldi procedure is still far cheaper than the full diagonalization method. General details of the iterative method can be found in the literature [107, 108].

The significant reduction in computational cost offered by this method was exploited in Papers I and II where matrices of size $\sim 10^5 \times 10^5$ we used and extracting as many as 20 to 1000 lowest eigenvalues. Note that self-consistent calculation is not possible with this method since high states above the energy gap are needed for self-consistency.

4.1.3 Expressions for relevant quantities in BdG formalism

The BdG formalism offers easy access to relevant quantities through the wave function amplitudes or coherence factors. Experimentally accessible quanti-

ties can then be calculated. Listed here are some of the quantities used in the analysis of materials studied in this Thesis.

Densities

Local density of states (LDOS) and Spin-polarized density of states (SPLDOS) are usually measured in scanning tunnelling microscopy and scanning tunnelling spectroscopy experiments.

$$\text{SPLDOS} : \rho_{i\alpha}(E) = \langle c^{\dagger}_{i\alpha} c_{i\alpha} \rangle = \sum_{\nu} \left[|u^{\nu}_{i\alpha}|^2 \, \delta\left(E - E^{\nu}\right) + |v^{\nu}_{i\alpha}|^2 \, \delta\left(E + E^{\nu}\right) \right] \tag{4.3a}$$

where α denotes spin.

$$\text{LDOS} : \rho_i(E) = \sum_{\alpha} \langle c^{\dagger}_{i\alpha} c_{i\alpha} \rangle = \sum_{\alpha} \rho_{i\alpha} \tag{4.3b}$$

$$\text{DOS} : \rho(E) = \sum_{i\alpha} \langle c^{\dagger}_{i\alpha} c_{i\alpha} \rangle = \sum_{i\alpha} \rho_{i\alpha} = \sum_{i} \rho_i \tag{4.3c}$$

Spin projection

Information about the spin can be obtained by projecting the eigenvector of each energy level ν on the spin in a particular direction [109, 110] i.e.

$$S^{\eta}_{i,\nu} = \sum_{j} \left\langle \psi^{\nu}_i \left(\tau^x_i \otimes \sigma^{\eta} \right) \psi^{\nu}_j \right\rangle \tag{4.4}$$

where $\tau(\sigma)$ are Pauli matrices in particle-hole(spin) spaces. For projection along x is,

$S^x_{i,\nu} = \left[\left(u^{\nu}_{i\uparrow} v^{\nu *}_{i\downarrow} + u^{\nu}_{i\uparrow} v^{\nu *}_{i\downarrow} \right) f_{\text{FD}}\left(\beta E^{\nu}\right) + \left(u^{\nu *}_{i\uparrow} v^{\nu}_{i\downarrow} + u^{\nu *}_{i\uparrow} v^{\nu}_{i\downarrow} \right) f_{\text{FD}}\left(-\beta E^{\nu}\right) \right]$

In a similar manner all the quantities listed in section 4.1.3, Eqs. (4.1), (4.3), (4.4), can be written in moment space by making appropriate Fourier transformations.

4.2 Spectral methods

The Arnoldi method reduces computational cost significantly when $\hat{H}_{\text{BdG}}$ is very large. However, some information about the system is lost because some states are not calculated, in this case the high energy states. What if $\hat{H}_{\text{BdG}}$ is large and one wants information of the full energy range? Alternative to diagonalization are the spectral methods which have computational time $\propto N$ instead of powers of N as in the case of diagonalization method. The symmetry of the function or basis, c_j, to be expanded determines the appropriate spectral method. In section 2.2.4 Fourier basis was used to expand c_j, which is a

type of spectral method. Fourier expansion is the natural spectral method for a periodic function but when the function is non-periodic and finite at the boundaries more appropriate expansions are Legendre and Chebychev series because they have finite intervals. In this Thesis the Chebychev polynomial expansion is used.

4.2.1 Chebyshev polynomial expansion

The Chebyshev method is a spectral method [111] which can be used to calculate the retarded Green's function $G_{ij}(\omega) = \langle \Psi_i | \left[\omega + i\eta - \hat{H}_{\mathrm{BdG}}\right]^{-1} | \Psi_j \rangle$, where $|\Psi_j\rangle$ is the eigenvector of the of the position operator at site j. Rather than direct inversion of the matrix, which is expensive, the Green's function is expanded in terms of Chebyshev polynomial. The coefficient of the nth expansion term is a_{ij}^n, and can be expressed in terms of the Chebyshev polynomial[1] $T_n\left(\tilde{H}_{\mathrm{BdG}}\right)$ [112, 113, 114, 115] as,

$$a_{ij}^n = \langle q_i^0 | T_n\left(\tilde{H}_{\mathrm{BdG}}\right) | q_j^0 \rangle = \langle q_i^0 | q_j^n \rangle \tag{4.5}$$

where $\tilde{H}_{\mathrm{BdG}}$ denotes the rescaled $\hat{H}_{\mathrm{BdG}}$ such that the eigenvalues of $\tilde{H}_{\mathrm{BdG}}$ falls in the interval $[-1,\ 1]$ which is the interval of normalization of the $T_n(x) = \cos(n \arccos(x))$. The vector $|q_j^0\rangle = |c_j\rangle = c_j^\dagger |\mathrm{vacuum}\rangle$ is a vector with an entry of unity at the position j while all other elements are zero.

The nth Chebyshev polynomial is obtained by the recurrence relation

$$\begin{aligned} &T_n(x) = 2xT_{n-1}(x) - T_{n-2}(x) \\ &T_0 = 1, \qquad T_1 = x. \end{aligned} \tag{4.6}$$

From Eq. (4.6) all higher order polynomials can be obtained. Thus, the first and nth order polynomial expansion of the position eigenvector in Eq. (4.5) are given by

$$\begin{aligned} &|q_j^1\rangle = \tilde{H}_{\mathrm{BdG}} |q_j^0\rangle, \\ &|q_j^n\rangle = T_n\left(\tilde{H}_{\mathrm{BdG}}\right) |q_j^0\rangle = 2\tilde{H}_{\mathrm{BdG}} |q_j^{n-1}\rangle - |q_j^{n-2}\rangle. \end{aligned} \tag{4.7}$$

The retarded Green's function is then obtained as

$$G_{ij}(\tilde{\omega}) = \frac{-2i}{\sqrt{1-\omega^2}} \sum_{n=0}^{\infty} \frac{a_{ij}^n e^{n \arccos(\tilde{\omega})}}{1+\delta_{0,n}}. \tag{4.8}$$

The denominator is obtained from normalization condition of the Chebyshev polynomials. The whole process can be seen as re-expressing the retarded

[1] T_n are Chebyshev polynomials of the first kind. Chebyshev polynomials of the second kind. $U_n(x)$ can also be used.

Green's function in terms of Chebyshev coefficients. Note that the local density of states (LDOS) is obtained as

$$\rho(\omega, i) = -\frac{1}{\pi}\mathrm{Im}\left[G_{ii}(\tilde{\omega})\right] \tag{4.9}$$

This method is very computationally cheap and permits simulations of systems with experimentally realistic parameters. This is because most of the operations involves summations, as seen in Eq. 4.8. The most expensive part is the last expression of Eq. (4.7) which involves multiplication of matrices and vectors. Using sparse multiplication will further speed up the calculation. From the form of Eq. (4.5) it is possible to extract the coefficients a_{ij}^n for a single site or a region of the lattice, and then obtain the LDOS on that site or a region of the lattice. This is the power of the Chebyshev polynomial expansion method. Thus, it should be noted that when the information of the full lattice is required the method may become computationally expensive.

The Chebyshev method is efficiently implemented in the TBTK code package [116]. In Paper IV, the Chebyshev method, with 10^4 coefficients in the expansion, is used to simulate superconducting graphene with lattice size of 1000×1000 giving $\hat{H}_{\mathrm{BdG}}$ matrix of size $\sim 10^6 \times 10^6$. This allowed the use of reasonable experimental parameters for graphene.

Part II:
Results

In this part the results in the papers leading to this Thesis are summarized. Details are available in Papers I-IV.

5. Studies of Majorana bound states via defects

5.1 Majorana bound states in real materials

As discussed in chapter 3, *p*-wave topological superconductors with Majorana bound states at the ends can be engineered in the laboratory by combining common ingredients, namely: superconductivity, spin-orbit coupling and magnetism. There are several ways of combining materials to realize effective 1D *p*-wave superconductor with Majorana bound states at its edges. Of these methods, two are prominent with several experimental reports.

In one approach, magnetic impurities are deposited to form a chain on a spin-orbit coupled superconductor [105, 117, 118], see figure 5.1. Signatures of Majorana bound states have been reported in experiments by depositing Fe atoms on Pb in the superconducting phase [33, 119, 120, 118]. In this method the magnetic impurities are ferromagnetic.Using this approach, in section 5.2, robustness of Majorana bound states to potential disorder is studied.

In another approach a semiconductor nanowire with strong Rashba spin-orbit coupling is proximitized to a conventional *s*-wave superconductor [121, 122, 123, 124, 125]. An external magnetic field is then applied. The magnetic field is used to drive the system from the trivial phase to a topological phase with Majorana bound states appearing at the ends of the nanowire [122, 123, 124]. Using this approach several experiments have reported signatures of Majorana bound states [32, 126].

5.2 PAPER I: Majorana bound states in ferromagnetic chains on conventional superconductors are robust against disorder

As explained in chapter 3, Majorana bound states are robust against local perturbations, due to their nonlocal and topological properties. In experiments to create Majorana bound states, the superconductor will contain some form of *defects*. For a hybrid superconductor-nanowire system it was shown that the base superconductor must be extremely clean in order to obtain well isolated Majorana bound states [42, 43]. Merely extending this result to magnetic chains in a superconductor would imply that Majorana bound states at the ends of magnetic chain are sensitive to disorder.

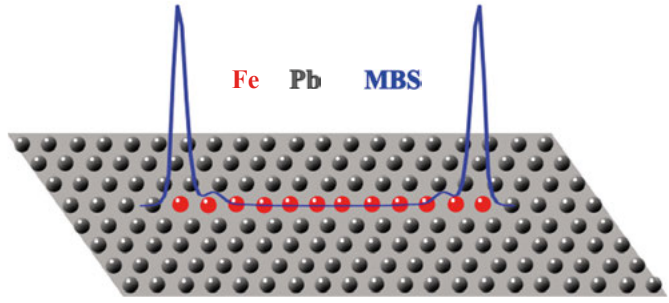

Figure 5.1. Schematic of a chain of magnetic impurities (Fe) on conventional spin-orbit coupled *s*-wave superconductor (Pb). The magnetic impurities give rise to an effective Zeeman term along the chain in the superconductor. The overall result is the appearance of Majorana bound states (MBS) at the edges of the magnetic chain. Details of the experiment can be found in Ref. [33].

Paper I in this Thesis investigates the effect of disorder on Majorana bound states on a chain of magnetic impurity deposited on a disordered *s*-wave superconductor. Figure 5.1 schematically depicts the experimental scenario simulated in Paper I. The total Hamiltonian is given by

$$H = H_{\mathrm{SC}} + H_{\mathrm{Z}} + H_{\mathrm{disorder}}, \tag{5.1}$$

where H_{SC} is the Hamiltonian of the base superconductor which is modeled with on-site *s*-wave superconductivity on a square lattice using the mean-field Hamiltonian described in Eqs. (2.4). Also, the superconductor has Rashba spin-orbit coupling, as this is the case for Pb(110) used in the experiment [33]. The order parameter Δ_i at lattice site i is calculated self-consistently with Eq. (2.5) using the full diagonalization method discussed in section 4.1.1. H_{Z} is the effective Zeeman effect which comes from the magnetic chain. The magnetic impurities in the chain are considered to be ferromagnetically aligned. Defects are introduced in the base superconductor through H_{disorder}. Disorder here is a random fluctuation of the chemical potential in the superconductor, that is a site dependent chemical potential. This type of disorder, also called Anderson disorder [22], is generated by charge inhomogeneities or puddle formation, which is inevitable in experiments. This disorder has the benefit of keeping the average chemical potential unchanged. Details of each term in the Hamiltonian are explicitly given in Paper I.

The results showed that Majorana bound states are very robust against disorder. Majorana bound states remain at zero energy until disorder is very strong. Using self-consistent calculations, Paper I shows that Majorana bound states are not susceptible to disorder as long as superconductivity is not destroyed. Paper I also shows that at very strong disorder strength Anderson's theorem, which states that *s*-wave superconductors are not susceptible to potential disorder, breaks down. This leads to local destruction of superconducting correlations in some regions in the superconductor. This destruction of

superconductivity is hidden in disorder averaged calculation. This is because after averaging over several disorder configurations the effect of disorder is washed out, almost completely, in disorder averaged quantities. Analysis of a single disorder configuration is more appropriate for experiments, since few samples are used in experiments, and it also yields the condition for Majorana bound state robustness in a disordered superconductor: Majorana bound states, in magnetic chains deposited on a conventional superconductor, remain stable as long as superconductivity is not destroyed. Details can be found in Paper I attached.

5.3 PAPER II: Majorana bound states versus trivial zero-energy states in nanowire junctions

Despite the advancement in the search for Majorana bound states there is still no consensus whether Majorana bound states have been observed or not. One reason for this controversy is because it was shown that trivial zero-energy states can appear due to chemical inhomogeneities and can attain quantized conductance, just like Majorana bound states [34]. Furthermore, it has been shown that when the coupling between the nanowire and superconductor is strong the energies of the nanowire are shifted and this will then have an effect on the topological transition point of the nanowire [71, 127]. In the strong coupling regime, which is experiemtally achieved by epitaxially growing the superconductor on the nanowire [128], it is important to study the full nanowire-superconductor system as a single entity in order to capture the experimental situation more accurately.

Paper II in this Thesis studies a nanowire proximitized to two finite 2D superconductors to form a superconductor-nanowire-superconductor junction. The result shows that the nanowire parameters are sensitive to the size of the superconductor, most sensitive of all is the induced chemical potential in the nanowire. Remarkably, just by tuning the width of the superconductor the induced chemical potential can fill or deplete the nanowire levels. Thus, the width of the superconductor dictates when the nanowire becomes a topological superconductor. Even more interesting is that different scenarios can be achieved at the junction by tuning the superconductor width. For instance the junction can form a quantum dot, depending on the width of the superconductor, which can attain zero energy. This is a spontaneous formation of zero-energy state. In an experiment these trivial zero-energy state can mimic Majorana bound states.

To distinguish between trivial zero-energy states and Majorana bound states the supercurrent is calculated, and the result shows that as the Zeeman interaction strength increases the supercurrent across the junction in the presence of

trivial zero-energy states undergoes a sign reversal, that is a $\pi-$shift, but such sign reversal is absent in the supercurrent when topological Majorana bound states are present at the junction. Thus, Paper II proposes supercurrent measurements as a tool for unambiguous detection and distinction between trivial zero-energy states and Majorana bound states. Details can be found in Paper II attached.

6. Studies of topological and unconventional superconductivity in graphene via defects

In this chapter a summary of the results obtained from studying superconductivity in graphene, or generally honeycomb lattice, is given.

Graphene has exotic electronic states [8, 9], and several many-body instabilities including superconductivity, have been predicted to exist in graphene. As discussed in section 2.5.3, the D_{6h} point group of the honeycomb lattice allows for several irreducible representations which implies that a vast variety of superconducting states are possible in graphene. Focusing on nearest-neighbor interaction in the spin-singlet channel, since spin-orbit coupling is negligible in graphene and higher order interaction strength has no qualitative effect [129], the linearized gap equation, Eq. 2.18, predicts that at T_c the possible nearest-neighbor superconducting states in graphene are degenerate unconventional nodal $d_{x^2-y^2}-$ and $d_{xy}-$waves belonging to the E_{2g} irreducible representation and conventional extended $s-$wave, s_{ext}, belonging to the A_{1g} irreducible representation, see Table 2.1 and appendix B.

Below T_c the honeycomb lattice favors equal complex admixture of the degenerate $d-$wave states to form a fully gapped chiral d-wave, i.e. a $d_{x^2-y^2} \pm id_{xy}-$wave superconducting state. The chiral d-wave state breaks time reversal symmetry through the complex nature of its superconducting order parameter. The chiral d-wave superconducting state has been predicted by several theoretical methods, including mean-field [11, 20], renormalization group [13] and functional renormalization group [12], to exist in the honeycomb lattice at doping levels close to the van Hove singularity. While the nodal d-wave states break the sixfold symmetry of the lattice, the chiral d-wave obey the lattice symmetry, however, it is a Class C topological superconducting state, (see Table 3.1) with topological invariant given by the Chern or winding number $N = \pm 2$, described in Eq. 3.2, respectively, for $d_{x^2-y^2} \pm id_{xy}$. The Chern number gives the chirality and the number of edge states, according to bulk-edge correspondence. *It should noted that chirality here refers to the complex nature of the order paramter, and should not be confused with the chiral symmetry of graphene which refers to the sublattice symmetry of graphene.* It has been shown that chiral d-wave superconductivity in graphene has two edge estates as expected from bulk-edge correspondence [129]. Further details of chiral d-wave superconducting state in doped graphene can be found in [20].

Considering effective nearest-neighbor electron-electron interaction at finite doping levels up to and beyond the van Hove singularity, both intrinsic

and proximity-induced superconductivity in graphene are studied by introducing defects. All the aforementioned superconducting states, especially the topological chiral d-wave state are studied. The results are summarized below.

6.1 PAPER III: Domain wall in chiral d-wave superconductor on the honeycomb lattice

The two possible chiral d-wave states, $d_{x^2-y^2}+id_{xy}$ and $d_{x^2-y^2}-id_{xy}$, are degenerate. Thus, a domain wall can form between these states. The domain wall is formed when the order parameter changes from $d_{x^2-y^2}+id_{xy}$-wave on one side of the lattice to $d_{x^2-y^2}-id_{xy}$-wave on the other side of the lattice. The domain wall is formed because of change in chirality across of the lattice. Figure 6.1(a) shows the spectral flow, obtain from Eq. (4.2), at the left edge, domain wall, and right edge. The spectral flow shows that there are two copropagating states per edge, and four copropagating states at the domain wall, Figure 6.1(a). The domain wall states occur as a consequence of the jump in the topological invariant from $+2$ to -2. This is consistent with prediction of bulk-edge correspondence as discussed in section 3.2. The flow is schematically shown in Figure 6.1(b). The flow is clockwise for $d_{x^2-y^2}+id_{xy}$ and anticlockwise $d_{x^2-y^2}-id_{xy}$. At the domain wall the flow is in the same direction.

Paper III carries out full self-consistents calculation of different domain walls in chiral d-wave superconducting graphene was carried out using full diagonalization method, discussed in section 4.1.1. The result shows that the domain wall energy have multiple minima as a function of the phase difference across the domain wall. The most favorable state is determined by the order parameter profile that has the minimum width around the domain wall, provided that it is not a sharp profile.

Although the most favorable domain wall orientation is doping dependent, it is not sensitive to the interaction strength. For doping levels below the van Hove singularity, the domain walls along the armchair edge are most favorable with no phase difference, while the domain walls along the zigzag edge are favored for doping above van Hove singularity now with a finite phase difference. There is no preference at the van Hove singularity. This behavior is attributed to the changes in the topology of the normal state of graphene with doping. Despite the sensitivity of the domain wall state to edge type, doping and phase difference the superconducting order parameter has a universal inverse relationship with the domain wall width, in agreement with phenomenological theory [77].

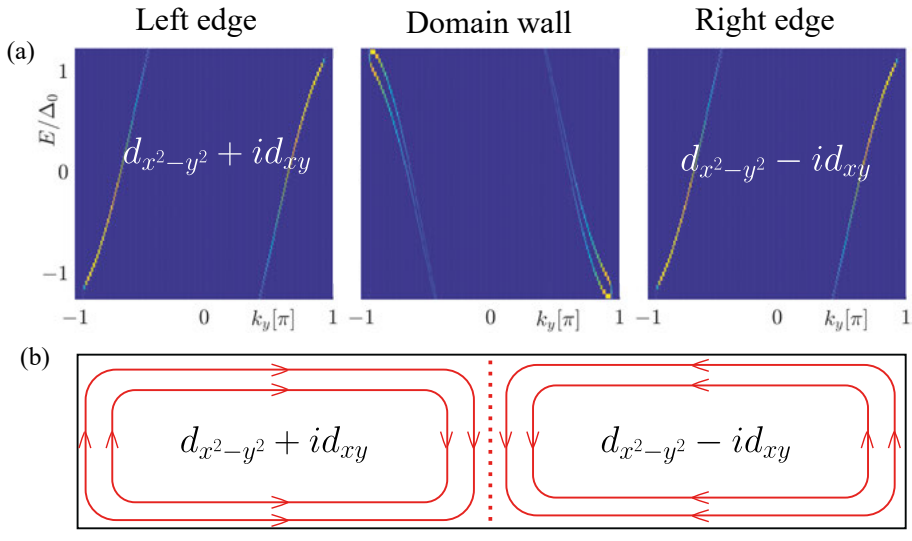

Figure 6.1. (a) Plot of the spectral function, $A(E,k_y,x)$ given in Eq. (4.2), at the boundaries of chiral d-wave superconductor on the honeycomb lattice. The left (right) side of the lattice has $d_{x^2-y^2}+id_{xy}-$ ($d_{x^2-y^2}-id_{xy}-$)wave superconducting states, so that a domain wall is formed at the middle of the lattice. The sign of the slope of the boundary states gives the direction of flow of the chiral edge states. There are four copropagating domain wall states, middle panel, but with flow opposite that of the edge states, left and right panels. A finite phase difference across the domain wall has been introduced to lift the degeneracy of the domain wall states. (b) Schematics of the flow of the boundary states. The degenerate edge states at each edge are copropagating and the domain wall states are also copropagating. Note that there are four domain wall states in agreement with the bulk-edge correspondence.

Chiral superconductors are expected to have domain wall states. This study then proposed that a finite differential conductance at zero bias within the bulk of superconductor is a feature of domain wall states. Details can be found in Paper III attached.

6.2 PAPER IV: Probing unconventional superconductivity in graphene via potential impurities

As discussed earlier, and in section 2.5.3, the honeycomb lattice allows for several possible superconducting states under several irreducible representations. Following an experiment where superconductivity was induced in graphene through proximity to a cuprate superconductor [18], in Paper IV all possible spin-singlet superconducting states, up to nearest-neighbor pairing, in graphene are studied using a single potential impurity. The system is mod-

eled using Eqs. (2.4) but adding a single potential impurity such that the total Hamiltonian is $\hat{H} = \hat{H}_{\mathrm{BdG}} + \hat{H}_{\mathrm{imp}}$, where $\hat{H}_{\mathrm{imp}}$ is single the impurity Hamiltonian. The result shows that a single potential impurity introduced on the graphene will aid the characterization of the superconducting states. To avoid interference with edge states, a large lattice size with experimentally realistic parameters is used. The calculation is carried out with Chebyshev polynomial expansion method, discussed in section 4.2.1.

A very interesting finding is that the normal state Dirac point still hosts a virtual bound state outside the superconducting gap. This supergap state is always present irrespective of the superconducting state and it has the same features as that of the impurity state in normal graphene. There are also subgap impurity resonance states, states within energy gap due to impurity, in the unconventional and topological superconducting states. These subgap states reveal the symmetry of the superconducting states in the spatial local density of states. The unconventional d-wave and chiral d-wave states show different patterns in real space when probed at impurity resonance energy. The Fourier transform of the local density of states [130, 131], known as the quasiparticle interference, also shows different patterns in the Brillouin zone.

Paper IV shows that introducing a single potential impurity into proximitized graphene in a scanning tunnelling spectroscopy or microscopy experiment will reveal the symmetry of the superconducting state induced in the graphene layer. Details can be found in Paper IV attached.

7. Conclusion and Outlook

The results of this Thesis show that defects can be powerful tools for studying topological superconductors, when properly controlled and manipulated. Using different types of defects this Thesis has successfully studied a range of topological superconductors.

The field of superconductivity is constantly growing. Novel materials with unconventional superconducting correlations, but lacking theoretical explanation at the moment, are found from time to time. Examples are the iron-based superconductors [132, 133, 134] and twisted bilayer graphene [60, 135] both of which have attracted a lot of attention since their discoveries. Multilayer graphene systems are very interesting materials because the low-energy dispersion is dependent on the stacking order. In the special case of ABC-stacked multilayer graphene [136] the low-energy bands are dispersionless at the Fermi energy, around the K-points, due to the topology of the system. The flat bands give rise to a large density at the Fermi energy, contrary to single layer graphene where there is no density of states at the Fermi energy due to the presence of a Dirac point. The presence of a large density of states suggests that ABC-stacked multilayer graphene might be prone to superconducting instability, albeit such superconducting state will have to compete with magnetism since density functional theory on a few layers and experiment on trilayers [137] predict a magnetic ground state. Another multilayer graphene system yet to be studied for superconductivity is biased bilayer graphene, which is a Bernal stacking of two graphene sheets but with one of the layers staggered i.e. the onsite energies in the two sublattices are different. Experimental results show a flat band around the K-points [138]. The presence of flat a band has led to speculations of unconventional superconductivity in the material, but there is no detailed study of superconductivity in the material at the moment.

Just as in graphene systems, a lot of activities are going on in the search for Majorana bound states. Although, current experimental set-ups have achieved a large induced gap, the strong coupling achieved have also resulted in detrimental effects such as reduction in spin-orbit coupling [39], large induced chemical potential in the nanowire [39, 71, 127], all of which can conspire to postpone the topological transition point to very large magnetic field values. It is therefore imperative to return to the weak coupling regime where the effect of the base superconductor on the parameters of the nanowire is negligible. The believe in the community is that the induced order parameter in this regime is small and thus the gap in the nanowire will be soft. But a detailed investigation may change this view.

With the tools at our disposal coupled with experienced gained from previous studies we hope to investigate the problems listed above and also to study other interesting systems.

8. Svensk sammanfattning

Defekter refererar generellt sett till objekt och strukturer som förhindrar en mjuk kontinuitet i ett material. En elektron i rörelse kan kollidera med en defekt och ändra sin rörelseriktning, vilket kallas för spridning, eller så kan elektronen fångas av defekten. I vanliga fall är defekter oönskade i material men då de introduceras avsiktligt och på ett kontrollerat sätt kan de användas som kraftfulla prober. Det finns många typer av defekter och deras påverkan på materialet beror på både defekten och materialet. Det vanligaste exemplet på en defekt är materialets kant där materialet tar slut (precis som en bordskant). Vad som händer vid ett materials kant beror på materialets natur. Ett annat exempel på en defekt är en orenhet, vilken är en främmande atom med andra egenskaper än de atomer som materialet består av. Elektroner som sprids mot en orenhet lämnar spår i materialet. Genom att studera dessa spår i materialet så kan materialets natur eller underligande fenomen visa sig. En knutpunkt, vilket är en annan form av orenhet, fungerar som en länk mellan material och tillåter att en ström flyter mellan olika material. Dessa exempel visar att defekter kan vara kraftfulla prober för att studera material.

När materialet som studeras är en supraledare (supraledare är material som leder elektrisk ström utan motstånd när de kyls ned till i närheten av den absoluta nollpunkten) så är defektens påverkan beroende på supraledarens natur. Den supraledande orderparametern (en storhet som har ett ändligt värde i den supraledande fasen men som är noll när materialet inte är supraledande och vilken skapar ett energigap mellan energinivåerna i supraledaren) bestämmer hur supraledaren svarar på en defekt. Beroende på supraledarens natur så kan defekter åstadkomma lågenergitillstånd inuti supraledarens energigap. Därför är det möjligt att genom att studera vissa defekter i en supraledare förutsäga egenskaperna hos lågenergitillstånden inuti gapet eller t.o.m. supraledarens natur. Ett material för vilket detta kan vara användbart är grafen.

Grafen består av kolatomer organiserade i ett hexagonalt mönster. Grafen är populärt på grund av dess exotiska egenskaper och potentiella teknologiska tillämpningar. På grund av sitt hexagonala mönster kan det ge upphov till flera olika supraledande tillstånd. Intressant nog ser de flesta av dessa tillstånd likadana ut vid experimentella mätningar på rent grafen. Det är därför svårt att avgöra experimentellt vilket supraledande tillstånd grafen har. I ett av projekten i denna avhandling har en potentiell orenhet introducerats i supraledande grafen och effekten av olika typer av möjliga supraledande tillstånd beräknas. Resultatet av denna studie visar att spåren av de spridda elektronerna

formar rumsliga mönster i den supraledande orederparametern för vart av de supraledande tillstånden. Kunskap om de rumsliga mönstren eller symmetrin för orderparametern innehåller hälften av informationen som behövs för att bestämma det supraledande tillståndet. Den andra halvan av informationen är antalet lågenergitillstånd. Genom att kombinera dessa två bitar av information föreslår detta projekt experiment som otvetydigt kan bestämma det supraledande tillståndet i grafen.

En speciell klass av exotiska supraledare som kallas topologiska supraledare innehåller nollenergitillstånd, vilka kallas för Majoranafermioner, vid dess kanter. De bundna Majoranatillstånden är okänsliga för defekter och har egenskaper som gör dem till lovande kandidater för qubitar (en qubit är en kvantmekanisk version av en bit i klassiska datorer) i feltolleranta kvantdatorer. Enorma ansträngningar har gått till att söka efter bundna Majoranatillstånd. I ett av projekten i denna avhandling har bundna Majoranatillstånd utsatta för stark oordning för att testa hur robusta de är mot defekter. Detta test utförs genom numeriska simuleringar av de förhållanden under vilka bundna Majoranatillstånd skapas i labboratorier. Resultaten visar att så länge materialet fortsätter att vara supraledande så påverkas de bundna Majoranatillstånden inte av oordning. Detta är goda nyheter eftersom stabilitet mot oordning garanterar att qubitar som skapats från bundna Majoranatillstånd kommer vara stabila.

Trotts deras stabilitet så finns det svårigheter att detektera bundna Majoranatillstånd i experiment. Det är nämligen möjligt för oönskade triviala nolltillstånd att framträda i experiment som är ämnade att skapa bundna Majoranatillstånd. Dessa triviala nolltillstånd kan imitera bundna Majoranatillstånd och skapa tvetydighet vid tolkningen av experimentella resultat. Denna utveckling skapar svårigheter gällande hur man skall särskilja mellan de triviala nolltillstånden och bundna Majoranatillstånd. Det är viktigt att det nolltillstånd som används för att skapa en qubit är ett bundet Majoranatillstånd eftersom qubiten annars kommer sakna sina topologiska egenskaper, vilket gör feltolleranta kvantberäkningar omöjliga. I ett av projekten i denna avhandling simuleras ett experimentellt scenario för att skapa ett bundet Majoranatillstånd. Genom att beräkna strömen genom en knutpunkt i supraledaren då ett magnetiskt fällt varieras så visar det sig att strömmen från ett trivialt nolltillstånd genomgår ett teckenbyte då det magnetiska fältet ändras, medan ett bundet Majoranatillstånd inte genomgår ett sådant teckenbyte. Detta projekt föreslår mätningar av strömmen genom knutpunkter i topologiska supraledare som ett verktyg för att särskilja mellan triviala nolltillstånd och bundna Majoranatillstånd.

På det hela taget undersöker denna avhandling möjligheten att undersöka supraledare med hjälp av olika sorters defekter. Slutsatsen av resultaten är att defekter mycket riktigt är kraftfulla verktyg för att studera supraledare och detta kan vara användbart för att realisera feltolleranta kvantdatorer.

Acknowledgement

I am grateful for being given the opportunity to conduct PhD research in a conducive environment like Uppsala University. I will like to give my heartfelt gratitude to my supervisor Annica Black-Schaffer, whose vast knowledge and experience I have benefited from. Her support and enthusiasm over the years of my studies have been crucial. Thanks Annica!

I thank my associate supervisor, Johan Nilson who has always been available for me. I also thank my collaborators, Kristofer Björson, Adrien Bouhon, Jorge Cayao, and Tomas Löthman for sharing their knowledge with me and for being fun to work with.

I am appreciative of Dushko Kumanovski, Mahdi Mashkoori, Chris Triola, Adrian Kantian, Paramita Dutta, and Johann Schmidt for several productive discussions. I am grateful to Jorge Cayao for taking the time to read the thesis and giving helpful feedbacks, and Kristofer Björson for helping to translate the Summary to Swedish.

I will like to thank everyone at Material Theory, Professors, seniors, Postdocs and PhD students, friends and members of Annica Black-Schaffer's group for sharing their knowledge with me. I have enjoyed the time I spent talking with several colleagues including Francesco Catalano, Juan David Aramillo, Andreas Theiler, Suhas Nahas, Fariborz Parhizgar, Anna Sinelnikova, Debmalya Chakraborty, and others.

My sincere gratitude goes to my family, especially Roseline and Ayobolaji, for their support throughout the study period. My friends outside Uppsala University have all been supportive, and I wish to thank you all.

Finally, I give thanks for Grace.

References

[1] P. G. de Gennes. *Superconductivity of Metals and Alloys*. W. A. Benjamin, Inc., New York, 1966.

[2] L. N. Cooper. Bound electron pairs in a degenerate Fermi gas. *Physical Review*, 104:1189–1190, 1956.

[3] M. Tinkham. *Introduction to Superconductivity*. Dover Publications, second edition, 2004.

[4] F. Steglich, J. Aarts, C. D. Bredl, W. Lieke, D. Meschede, W. Franz, and H. Schäfer. Superconductivity in the presence of strong Pauli paramagnetism: $Cecu_2si_2$. *Physical Review Letters*, 43:1892–1896, 1979.

[5] J. G. Bednorz and K. A. Müller. Possible high T_c superconductivity in the Ba-La-Cu-O system. *Zeitschrift für Physik B Condensed Matter*, 64(2):189–193, 1986.

[6] S. Uchida. *High Temperature Superconductivity: The Road to Higher Critical Temperature*, volume 213. Springer, Springer Tracts in Materials Science, 2014.

[7] B. D. White, J. D. Thompson, and M. B. Maple. Unconventional superconductivity in heavy-fermion compounds. *Physica C: Superconductivity and its Applications*, 514:246–278, 2015.

[8] K. S. Novoselov, A. K. Geim, S. V. Morozov, D. Jiang, Y. Zhang, S. V. Dubonos, I. V. Grigorieva, and A. A. Firsov. Electric field effect in atomically thin carbon films. *Science*, 306(5696):666–669, 2004.

[9] A. H. C. Neto, F. Guinea, N. M. R. Peres, K. S. Novoselov, and A. K. Geim. The electronic properties of graphene. *Review of Modern Physics*, 81:109–162, 2009.

[10] T. O. Wehling, A. M. Black-Schaffer, and A. V. Balatsky. Dirac materials. *Advances in Physics*, 63(1):1–76, 2014.

[11] A. M. Black-Schaffer and S. Doniach. Resonating valence bonds and mean-field d-wave superconductivity in graphite. *Physical Review B*, 75:134512, 2007.

[12] M. L. Kiesel, C. Platt, W. Hanke, D. A. Abanin, and R. Thomale. Competing many-body instabilities and unconventional superconductivity in graphene. *Physical Review B*, 86:020507, 2012.

[13] R. Nandkishore, L. S. Levitov, and A. V. Chubukov. Chiral superconductivity from repulsive interactions in doped graphene. *Nature Physics*, 8(2):158–163, 2012.

[14] P. Rosenzweig, H. Karakachian, S. Link, K. Küster, and U. Starke. Tuning the doping level of graphene in the vicinity of the van Hove singularity via ytterbium intercalation. *Physical Review B*, 100:035445, Jul 2019.

[15] P. Rosenzweig, H. Karakachian, D. Marchenko, K. Küster, and U. Starke. Overdoping graphene beyond the van Hove singularity. *Physical Review Letters*, 125:176403, 2020.

[16] H. B. Heersche, P. Jarillo-Herrero, Jeroen B. Oostinga, L. M. K. Vandersypen, and A. F. Morpurgo. Bipolar supercurrent in graphene. *Nature*, 446(7131):56–59, 2007.

[17] J. L. McChesney, A. Bostwick, T. Ohta, T. Seyller, K. Horn, J. González, and E. Rotenberg. Extended van Hove singularity and superconducting instability in doped graphene. *Physical Review Letters*, 104(13):136803, 2010.

[18] A. Di Bernardo, O. Millo, M. Barbone, H. Alpern, Y. Kalcheim, U. Sassi, A. K. Ott, D. De Fazio, D. Yoon, M. Amado, A. C. Ferrari, J. Linder, and J. W. A. Robinson. *p*-wave triggered superconductivity in single-layer graphene on an electron-doped oxide superconductor. *Nature communications*, 8(14024):1–9, 2017.

[19] D. Perconte, K. Seurre, V. Humbert, C. Ulysse, A. Sander, J. Trastoy, V. Zatko, F. Godel, P. R. Kidambi, S. Hofmann, X. P. Zhang, D. Bercioux, F. S. Bergeret, B. Dlubak, P. Seneor, and Javier E. Villegas. Long-range propagation and interference of *d*-wave superconducting pairs in graphene. *Physical Review Letters*, 125:087002, Aug 2020.

[20] A. M. Black-Schaffer and C. Honerkamp. Chiral *d*-wave superconductivity in doped graphene. *Journal of Physics: Condensed Matter*, 26(42):423201, 2014.

[21] A. V. Balatsky, I. Vekhter, and Jian-Xin Zhu. Impurity-induced states in conventional and unconventional superconductors. *Review of Modern Physics*, 78:373–433, 2006.

[22] W. P. Anderson. Theory of dirty superconductors. *Journal of Physics and Chemistry of Solids*, 11:26–30, 1969.

[23] O. A. Awoga and A. M. Black-Schaffer. Probing unconventional superconductivity in proximitized graphene by impurity scattering. *Physical Review B*, 97:214515, 2018.

[24] N. Read and D. Green. Paired states of fermions in two dimensions with breaking of parity and time-reversal symmetries and the fractional quantum hall effect. *Physical Review B*, 61(15):10267, 2000.

[25] L. Fu and C. L. Kane. Superconducting proximity effect and Majorana fermions at the surface of a topological insulator. *Physical Review Letters*, 100:096407, 2008.

[26] M. Sato, Y. Takahashi, and S. Fujimoto. Non-Abelian topological order in *s*-wave superfluids of ultracold fermionic atoms. *Physical Review Letters*, 103:020401, 2009.

[27] G. E. Volovik. On edge states in superconductors with time inversion symmetry breaking. *Journal of Experimental and Theoretical Physics Letters*, 66:522, 1997.

[28] M. Z. Hasan and C. L. Kane. Colloquium: Topological insulators. *Review of Modern Physics*, 82:3045–3067, 2010.

[29] X.-L. Qi and S.-C. Zhang. Topological insulators and superconductors. *Review of Modern Physics*, 83(4):1057, 2011.

[30] G. M. Graf and M. Porta. Bulk-edge correspondence for two-dimensional topological insulators. *Communication in Mathematical Physics*, 324(3):851–895, 2013.

[31] O. A. Awoga, A. Bouhon, and A. M. Black-Schaffer. Domain walls in a chiral *d*wave superconductor on the honeycomb lattice. *Physical Review B*,

96:014521, 2017.
[32] K. Mourik, V.and Zuo, S. M. Frolov, S. R. Plissard, E. P. A. M. Bakkers, and L. P. Kouwenhoven. Signatures of Majorana fermions in hybrid superconductor-semiconductor nanowire devices. *Science*, 336(6084):1003–1007, 2012.
[33] S. Nadj-Perge, I. K. Drozdov, J. Li, H. Chen, S. Jeon, J. Seo, A. H. MacDonald, B. A. Bernevig, and A. Yazdani. Observation of Majorana fermions in ferromagnetic atomic chains on a superconductor. *Science*, 346(6209):602–607, 2014.
[34] Chun-Xiao Liu, Jay D. Sau, Tudor D. Stanescu, and S. Das Sarma. Andreev bound states versus Majorana bound states in quantum dot-nanowire-superconductor hybrid structures: Trivial versus topological zero-bias conductance peaks. *Physical Review B*, 96:075161, 2017.
[35] A. Vuik, B. Nijholt, A. R. Akhmerov, and M. Wimmer. Reproducing topological properties with quasi-Majorana states. *SciPost Physics*, 7:61, 2019.
[36] Elsa Prada, Pablo San-Jose, Michiel W. A. de Moor, Attila Geresdi, Eduardo J. H. Lee, Jelena Klinovaja, Daniel Loss, Jesper Nygård, Ramón Aguado, and Leo P. Kouwenhoven. From Andreev to Majorana bound states in hybrid superconductor-semiconductor nanowires. *Nature Reviews Physics*, 2020.
[37] K. T. Law, Patrick A. Lee, and T. K. Ng. Majorana fermion induced resonant andreev reflection. *Physical Review Letters*, 103:237001, 2009.
[38] O. A. Awoga, K. Björnson, and A. M. Black-Schaffer. Disorder robustness and protection of Majorana bound states in ferromagnetic chains on conventional superconductors. *Physical Review B*, 95(18):184511, 2017.
[39] Oladunjoye A. Awoga, Jorge Cayao, and Annica M. Black-Schaffer. Supercurrent detection of topologically trivial zero-energy states in nanowire junctions. *Physical Review Letters*, 123:117001, 2019.
[40] A. Y. Kitaev. Unpaired Majorana fermions in quantum wires. *Physics-Uspekhi*, 44(10S):131, 2001.
[41] Chetan Nayak, Steven H. Simon, Ady Stern, Michael Freedman, and Sankar Das Sarma. Non-abelian anyons and topological quantum computation. *Review of Modern Physics*, 80:1083–1159, 2008.
[42] H.-Y. Hui, J. D. Sau, and S. Das Sarma. Bulk disorder in the superconductor affects proximity-induced topological superconductivity. *Physical Review B*, 92:174512, 2015.
[43] W. S. Cole, J. D. Sau, and S. Das Sarma. Proximity effect and Majorana bound states in clean semiconductor nanowires coupled to disordered superconductors. *Physical Review B*, 94(14):140505, 2016.
[44] P. San-Jose, J. L. Lado, R. Aguado, F. Guinea, and J. Fernández-Rossier. Majorana zero modes in graphene. *Physical Review X*, 5:041042, 2015.
[45] Michael Hell, Karsten Flensberg, and Martin Leijnse. Distinguishing Majorana bound states from localized Andreev bound states by interferometry. *Physical Review B*, 97:161401, 2018.
[46] Constantin Schrade and Liang Fu. Andreev or Majorana, Cooper finds out. *arXiv:1809.06370*, 2018.
[47] Konstantin Yavilberg, Eran Ginossar, and Eytan Grosfeld. Differentiating Majorana from Andreev bound states in a superconducting circuit. *Physical*

Review B, 100:241408, 2019.
[48] Vivien Perrin, Marcello Civelli, and Pascal Simon. Discriminating Majorana bound states by tunneling shot-noise tomography, 2020.
[49] H. K. Onnes. The resistance of pure mercury at helium temperatures. *Communications from the Laboratory of Physics at the University of Leiden*, 12:120+, 1911.
[50] W. Meissner and R. Ochsenfeld. Ein neuer effekt bei eintritt der supraleitfähigkeit. *Naturwissenschaften*, 21(44):787–788, 1933.
[51] F. London and H. London. The electromagnetic equations of the supraconductor. *Proceedings of the Royal Society (London) A: Mathematical, Physical and Engineering Sciences*, 149(866):71–88, 1935.
[52] A. B. Pippard. An experimental and theoretical study of the relation between magnetic field and current in a superconductor. *Proceedings of the Royal Society (London) A: Mathematical, Physical and Engineering Sciences*, 216(1127):547–568, 1953.
[53] T. E. Faber and A. B. Pippard. The penetration depth and high-frequency resistance of superconducting aluminium. *Proceedings of the Royal Society (London) A: Mathematical, Physical and Engineering Sciences*, 231(1186):336–353, 1955.
[54] V. L. Ginzburg and L. D. Landau. On the theory of superconductivity. *Zhurnal Éksperimental'noĭ i Teoreticheskoĭ Fiziki*, 20:1064–1082, 1950.
[55] H. Fröhlich. Theory of the superconducting state. i. the ground state at the absolute zero of temperature. *Physical Review*, 79:845–856, 1950.
[56] John Bardeen and David Pines. Electron-phonon interaction in metals. *Phys. Rev.*, 99:1140–1150, 1955.
[57] J. Bardeen, L. N. Cooper, and J. R. Schrieffer. Microscopic theory of superconductivity. *Physical Review*, 106:162–164, 1957.
[58] J. Bardeen, L. N. Cooper, and J. R. Schrieffer. Theory of superconductivity. *Physical Review*, 108:1175–1204, 1957.
[59] G. E. Volovik and L. P. Gor'kov. Superconducting classes in heavy-fermion systems. *Journal of Experimental and Theoretical Physics*, 61(4):843–854, 1985.
[60] Y. Cao, V. Fatemi, S. Fang, K. Watanabe, T. Taniguchi, E. Kaxiras, and P. Jarillo-Herrero. Unconventional superconductivity in magic-angle graphene superlattices. *Nature*, 556(7699):43, 2018.
[61] E. Majorana. Teoria simmetrica dell'elettrone e del positrone. *Il Nuovo Cimento*, 14(4):171, 1937.
[62] A. F. Andreev. The thermal conductivity of the intermediate state in superconductors. *Journal of Experimental and Theoretical Physics*, 19(5):1228, 1964.
[63] A. I. Buzdin. Proximity effects in superconductor-ferromagnet heterostructures. *Review of Modern Physics*, 77:935–976, 2005.
[64] P. Coleman. *Introduction to many-body physics*. Cambridge University Press, first edition, 2015.
[65] Y. Nambu. Quasi-particles and gauge invariance in the theory of superconductivity. *Physical Review*, 117:648–663, 1960.
[66] N. N. Bogoljubov. A new method in the theory of superconductivity. *Journal*

of Experimental and Theoretical Physics, 7(1):41–46, 1958.
[67] J. G. Valatin. Comments on the theory of superconductivity. *Il Nuovo Cimento*, 7(6):843–857, 1958.
[68] P. G. de Gennes. Boundary effects in superconductors. *Review of Modern Physics*, 36:225–237, 1964.
[69] A. M. Black-Schaffer and A. V. Balatsky. Proximity-induced unconventional superconductivity in topological insulators. *Physical Review B*, 87:220506, 2013.
[70] R. M. Lutchyn, E. P. A. M. Bakkers, L. P. Kouwenhoven, P. Krogstrup, C. M. Marcus, and Y. Oreg. Majorana zero modes in superconductor-semiconductor heterostructures. *Nature Review Materials*, 3:52, 2018.
[71] Christopher Reeg, Daniel Loss, and Jelena Klinovaja. Metallization of a Rashba wire by a superconducting layer in the strong-proximity regime. *Physical Review B*, 97:165425, 2018.
[72] M. Tinkham. *Group Theory and Quantum Mechanics*. Dover Publications, 2003.
[73] M. S. Dresselhaus, G. Dresselhaus, and A. Jorio. *Group theory: Application to the physics of condensed matter*. Springer-Verlag, 2008.
[74] Character tables for chemically important point groups. `http://symmetry.jacobs-university.de`. Accessed: 2018-11-13.
[75] Point group symmetry character tables. `http://www.webqc.org/symmetry.php`. Accessed: 2018-11-13.
[76] Symmetry resources at Otterbein University. `http://symmetry.otterbein.edu`. Accessed: 2018-11-13.
[77] M. Sigrist and K. Ueda. Phenomenological theory of unconventional superconductivity. *Review of Modern Physics*, 63:239–311, Apr 1991.
[78] P. V. Mineev and K. V. Samokhin. *Introduction to unconventional superconductivity*. Gordon and Breach Science Publishers, 1999.
[79] M. Mashkoori, K. Björnson, and A. M. Black-Schaffer. Impurity bound states in fully gapped d-wave superconductors with subdominant order parameters. *Scientific Reports*, 7:44107, 2017.
[80] A. T. Rømer, D. D. Scherer, I. M. Eremin, P. J. Hirschfeld, and B. M. Andersen. Knight shift and leading superconducting instability from spin fluctuations in Sr_2RuO_4. *Physical Review Letters*, 123:247001, 2019.
[81] AP Mackenzie. A personal perspective on the unconventional superconductivity of Sr_2RuO_4. *Journal of Superconductivity and Novel Magnetism*, 33(1):177–182, 2020.
[82] A. P. Mackenzie and Y. Maeno. The superconductivity of Sr_2RuO_4 and the physics of spin-triplet pairing. *Review of Modern Physics*, 75(2):657, 2003.
[83] A. Bouhon and M. Sigrist. Influence of the domain walls on the Josephson effect in Sr_2RuO_4. *New Journal of Physics*, 12(4):043031, 2010.
[84] C. Kallin. Chiral p-wave order in Sr_2RuO_4. *Reports on Progress in Physics*, 75(4):042501, 2012.
[85] C. Kallin and J. Berlinsky. Chiral superconductors. *Reports on Progress in Physics*, 79(5):054502, 2016.
[86] A. Pustogow, Yongkang Luo, A. Chronister, Y. S. Su, D. A. Sokolov, F. Jerzembeck, A. P. Mackenzie, C. W. Hicks, N. Kikugawa, S. Raghu, E. D.

Bauer, and S. E. Brown. Constraints on the superconducting order parameter in Sr_2RuO_4 from oxygen-17 nuclear magnetic resonance. *Nature*, 574(7776):72–75, 2019.

[87] S. H. Pan, E. W. Hudson, K. M. Lang, H. Eisaki, S. Uchida, and J. C. Davis. Imaging the effects of individual zinc impurity atoms on superconductivity in $Bi_2Sr_2CaCu_2O_{8+\delta}$. *Nature*, 403(6771):746, 2000.

[88] E. W. Hudson, K. M. Lang, V. Madhavan, S. H. Pan, H. Eisaki, S. Uchida, and J. C. Davis. Interplay of magnetism and hight_c superconductivity at individual ni impurity atoms in $Bi_2Sr_2CaCu_2O_{8+\delta}$. *Nature*, 411(6840), 2001.

[89] Øystein Fischer, Martin Kugler, Ivan Maggio-Aprile, Christophe Berthod, and Christoph Renner. Scanning tunneling spectroscopy of high-temperature superconductors. *Review of Modern Physics*, 79:353–419, Mar 2007.

[90] B. B. Zhou, S. Misra, E. H. da Silva Neto, P. Aynajian, R. E. Baumbach, J. D. Thompson, E. D. Bauer, and .i Yazdani. Visualizing nodal heavy fermion superconductivity in $CeCoIn_5$. *Nature*, 9(8):474, 2013.

[91] K. Leijnse, M.and Flensberg. Introduction to topological superconductivity and Majorana fermions. *Semiconductor Science and Technology*, 27(12):124003, 2012.

[92] B. A. Bernevig and T. L. Hughes. *Topological insulators and topological superconductors*. Princeton university press, 2013.

[93] M. Sato and Y. Ando. Topological superconductors: A review. *Reports on Progress in Physics*, 80(7):076501, 2017.

[94] R. Aguado. Majorana quasiparticles in condensed matter. *La Rivista del Nuovo Cimento*, 40:1, 2017.

[95] A. Altland and M. R. Zirnbauer. Nonstandard symmetry classes in mesoscopic normal-superconducting hybrid structures. *Physical Review B*, 55:1142–1161, 1997.

[96] C. Nash and S. Siddharta. *Topology and Geometry for Physists*. Dover Publications, Inc. New York., 1983.

[97] A. P. Schnyder, S. Ryu, A. Furusaki, and A. W. W. Ludwig. Classification of topological insulators and superconductors in three spatial dimensions. *Physical Review B*, 78:195125, 2008.

[98] Andreas W W Ludwig. Topological phases: classification of topological insulators and superconductors of non-interacting fermions, and beyond. *Physica Scripta*, T168:014001, dec 2015.

[99] M. V. Berry. Quantal phase factors accompanying adiabatic changes. *Proceedings of the Royal Society (London) A: Mathematical, Physical and Engineering Sciences*, 392(1802):45–57, 1984.

[100] Y. Tanaka, M. Sato, and N. Nagaosa. Symmetry and topology in superconductors–odd-frequency pairing and edge states–. *Journal of the Physical Society of Japan*, 81(1):011013, 2011.

[101] K. V. Klitzing, G. Dorda, and M. Pepper. New method for high-accuracy determination of the fine-structure constant based on quantized Hall resistance. *Phys. Rev. Lett.*, 45:494–497, 1980.

[102] R. B. Laughlin. Quantized hall conductivity in two dimensions. *Physical Review B*, 23:5632–5633, 1981.

[103] F. Wilczek. Majorana returns. *Nature Physics*, 5(9):614–618, 2009.

[104] S. R. Elliott and M. Franz. Colloquium: Majorana fermions in nuclear, particle, and solid-state physics. *Review of Modern Physics*, 87(1):137, 2015.
[105] S. Nadj-Perge, I. K. Drozdov, B. A. Bernevig, and A. Yazdani. Proposal for realizing Majorana fermions in chains of magnetic atoms on a superconductor. *Physical Review B*, 88(2):020407, 2013.
[106] S. Das Sarma, M. Freedman, and C. Nayak. Majorana zero modes and topological quantum computation. *Npj Quantum Information*, 1:15001, 2015.
[107] W. E. Arnoldi. The principle of minimized iterations in the solution of the matrix eigenvalue problem. *Quarterly of applied mathematics*, 9(1):17–29, 1951.
[108] C. Lanczos. An iteration method for the solution of the eigenvalue problem of linear differential and integral operators1. *Journal of Research of the National Bureau of Standards*, 45(4), 1950.
[109] Doru Sticlet, Cristina Bena, and Pascal Simon. Spin and majorana polarization in topological superconducting wires. *Physical Review Letters*, 108:096802, 2012.
[110] Marcel Serina, Daniel Loss, and Jelena Klinovaja. Boundary spin polarization as a robust signature of a topological phase transition in Majorana nanowires. *Physical Review B*, 98:035419, 2018.
[111] John P. Boyd. *Chebyshev and Fourier Spectral Methods*. Dover Publications, Inc., 2000.
[112] A. Weiße, G. Wellein, A. Alvermann, and H. Fehske. The kernel polynomial method. *Review of Modern Physics*, 78:275–306, Mar 2006.
[113] L. Covaci, F. M. Peeters, and M. Berciu. Efficient numerical approach to inhomogeneous superconductivity: The Chebyshev-Bogoliubov-de- Gennes method. *Physical Review Letters*, 105:167006, 2010.
[114] L. Covaci and F. M. Peeters. Superconducting proximity effect in graphene under inhomogeneous strain. *Physical Review B*, 84:241401(R), Dec 2011.
[115] K. Björnson. *Topological band theory and Majorana fermions : With focus on self-consistent lattice models*. PhD thesis, Uppsala University, Sweden., 2016.
[116] K. Björnson. dafer45/TBTK2017_09_26: Original version. `https://doi.org/10.5281/zenodo.997267`, September 2017.
[117] M. Sato, Y. Takahashi, and S. Fujimoto. Non-Abelian topological orders and Majorana fermions in spin-singlet superconductors. *Physical Review B*, 82(13):134521, 2010.
[118] R. Pawlak, M. Kisiel, J. Klinovaja, T. Meier, S. Kawai, T. Glatzel, D. Loss, and E.t Meyer. Probing atomic structure and Majorana wavefunctions in mono-atomic Fe chains on superconducting Pb surface. *Npj Quantum Information*, 2:16035, 2016.
[119] M. Ruby, F. Pientka, Y. Peng, F. von Oppen, B. W. Heinrich, and K. J. Franke. End states and subgap structure in proximity-coupled chains of magnetic adatoms. *Physical Review Letters*, 115(19):197204, 2015.
[120] B. E. Feldman, M. T. Randeria, J. Li, S. Jeon, Y. Xie, Z. Wang, I. K. Drozdov, B. A. Bernevig, and A. Yazdani. High resolution studies of the Majorana atomic chain platform. *Nature Physics*, 13:286, 2017.
[121] J. D. Sau, S. Tewari, R. M. Lutchyn, T. D. Stanescu, and S. Das Sarma. Non-Abelian quantum order in spin-orbit-coupled semiconductors: Search for

topological Majorana particles in solid-state systems. *Physical Review B*, 82:214509, 2010.
[122] R. M. Lutchyn, J. D. Sau, and S. Das Sarma. Majorana fermions and a topological phase transition in semiconductor-superconductor heterostructures. *Physical Review Letters*, 105(7):077001, 2010.
[123] J. Alicea. New directions in the pursuit of Majorana fermions in solid state systems. *Reports on Progress in Physics*, 75(7):076501, 2012.
[124] C. W. J. Beenakker. Search for Majorana fermions in superconductors. *Annual Review of Condensed Matter Physics*, 4:113–136, 2013.
[125] T. D. Stanescu and S. Tewari. Majorana fermions in semiconductor nanowires: fundamentals, modeling, and experiment. *Journal of Physics: Condensed Matter*, 25(23):233201, 2013.
[126] A. Das, Y. Ronen, Y. Most, Y. Oreg, M. Heiblum, and H. Shtrikman. Zero-bias peaks and splitting in an Al–InAs nanowire topological superconductor as a signature of Majorana fermions. *Nature Physics*, 8(12):887, 2012.
[127] Christopher Reeg, Daniel Loss, and Jelena Klinovaja. Finite-size effects in a nanowire strongly coupled to a thin superconducting shell. *Physical Review B*, 96:125426, 2017.
[128] W Chang, SM Albrecht, TS Jespersen, Ferdinand Kuemmeth, P Krogstrup, J Nygård, and CM Marcus. Hard gap in epitaxial semiconductor–superconductor nanowires. *Nature Nanotechnology*, 10(3):232–236, 2015.
[129] A. M. Black-Schaffer. Edge properties and Majorana fermions in the proposed chiral d-wave superconducting state of doped graphene. *Physical Review Letters*, 109:197001, 2012.
[130] G. M. Rutter, J. N. Crain, N. P. Guisinger, T. Li, P. N. First, and J. A. Stroscio. Scattering and interference in epitaxial graphene. *Science*, 317(5835):219–222, 2007.
[131] Julia Tesch, Philipp Leicht, Felix Blumenschein, Luca Gragnaniello, Anders Bergvall, Tomas Löfwander, and Mikhail Fonin. Impurity scattering and size quantization effects in a single graphene nanoflake. *Physical Review B*, 95:075429, 2017.
[132] Yoichi Kamihara, Hidenori Hiramatsu, Masahiro Hirano, Ryuto Kawamura, Hiroshi Yanagi, Toshio Kamiya, and Hideo Hosono. Iron-based layered superconductor: Laofep. *Journal of the American Chemical Society*, 128(31):10012–10013, 2006.
[133] M. Abdel-Hafiez, J. Ge, A. N. Vasiliev, D. A. Chareev, J. Van de Vondel, V. V. Moshchalkov, and A. V. Silhanek. Temperature dependence of lower critical field $H_{c1}(t)$ shows nodeless superconductivity in fese. *Physical Review B*, 88:174512, 2013.
[134] Qisi Wang, Yao Shen, Bingying Pan, Yiqing Hao, Mingwei Ma, Fang Zhou, P. Steffens, K. Schmalzl, T. R. Forrest, M. Abdel-Hafiez, and et al. Strong interplay between stripe spin fluctuations, nematicity and superconductivity in fese. *Nature Materials*, 15(2):159–163, 2015.
[135] Y. Cao, V. Fatemi, A. Demir, S. Fang, S. L. Tomarken, J. Y. Luo, J. D. Sanchez-Yamagishi, K. Watanabe, T. Taniguchi, E. Kaxiras, R.C. Ashoori, and P. Jarillo-Herrero. Correlated insulator behaviour at half-filling in magic-angle

graphene superlattices. *Nature*, 556(7699):80, 2018.
[136] Henry Solomon Lipson and A. R. Stokes. The structure of graphite. *Proceedings of the Royal Society (London) A: Mathematical, Physical and Engineering Sciences*, 181:101–105, 1942.
[137] Y Lee, D Tran, K Myhro, J Velasco, N Gillgren, CN Lau, Y Barlas, JM Poumirol, D Smirnov, and F Guinea. Competition between spontaneous symmetry breaking and single-particle gaps in trilayer graphene. *Nature communications*, 5(1):1–5, 2014.
[138] D. Marchenko, D. V. Evtushinsky, E. Golias, A. Varykhalov, Th. Seyller, and O. Rader. Extremely flat band in bilayer graphene. *Science Advances*, 4(11):aau0059, 2018.

Appendix A.
Derivation of the linearized gap equation

To arrive at Eq. (2.18) in the main text the following steps are followed:

1. The orbital basis $c-$operators are written in terms of band basis $a-$operators as
$$c_{ik\alpha} = \sum_{\bar{r}} \hat{S}_i^{\bar{r}} a_{k\bar{r}\alpha} \tag{A1}$$
where the unitary matrix $\hat{S} = \sum_{\bar{r}i} \hat{S}_i^{\bar{r}}$ diagonalizes the normal state Hamiltonian. This is substituted into Eq. (2.14) and Eq. (2.15).
2. The interacting density matrix ρ is expanded in terms of the noninteracting density matrix, $\rho_0 = e^{-\beta H_0}$, up to first order in interaction term so that
$$\rho = e^{-\beta H_0} - e^{-\beta H_0} \int_0^\beta \mathrm{d}\beta' e^{\beta' H_0} H_\Delta e^{-\beta' H_0} \tag{A2}$$
Here H_Δ is interacting part of Eq. (2.14) in the band basis, $a_{k\bar{r}\alpha}$.
3. Apply Baker-Campbell-Hausdorff formula, namely $e^A B e^{-A} = B + [A,B] + \frac{1}{2!}[A,[A,B]] + \cdots$ to calculate the density matrix obtained in step 2 above.
4. From statistical mechanics use that $\langle A \rangle = \mathrm{Tr}(\rho A)$ in new self-consistent equation in band basis $a_{k\bar{r}\alpha}$, noting that $\mathrm{Tr}\,(\rho_0 A) = 0$.
5. Finally, apply Wick's theorem $\langle A^\dagger B^\dagger C D \rangle_0 = \langle A^\dagger D \rangle_0 \langle B^\dagger C \rangle_0 - \langle A^\dagger C \rangle_0 \langle B^\dagger D \rangle_0$ to obtain the averages.

Note that $\tanh\left(\frac{\beta \xi_{\bar{r}}(k)}{2}\right) + \tanh\left(\frac{\beta \xi_{\bar{s}}(-k)}{2}\right) = \frac{\sinh[\xi_{\bar{s}}(k) + \xi_{\bar{r}}(k)]}{\cosh[\xi_{\bar{s}}(k)]\cosh[\xi_{\bar{r}}(k)]}$

Appendix B.
Spin-singlet nearest neighbor superconductivity in graphene

Considering chemical potential, μ, and nearest-neighbor hopping of strength, t, between sublattices A and B, the normal state Hamiltonian of graphene is given by

$$\hat{H}_0 = \begin{pmatrix} \mu & \varepsilon_k \\ \varepsilon_k^* & \mu \end{pmatrix}, \tag{B1}$$

where $\varepsilon_k = -t\sum_a e^{ik\cdot a}$ and $a = \begin{pmatrix} a_1 a_2 a_3 \end{pmatrix}$ are the bond direction vectors, see figure B1. Diagonalizing $\hat{H}_0$ gives the eigenvalues as $\xi_\pm(k) = \mu \pm |\varepsilon_k|$ with the corresponding eigenvectors making up the columns of the unitary matrix

$$\hat{S} = \sum_{r=A,B}\sum_{\bar{r}=\pm} \hat{S}_r^{\bar{r}} = \frac{1}{\sqrt{2}} \begin{pmatrix} 1 & 1 \\ -e^{-i\phi_k} & e^{-i\phi_k} \end{pmatrix} \tag{B2}$$

where $\phi_k = \arg(\varepsilon_k)$. Considering nearest-neighbor spin-singlet superconductivity, substituting $\xi_\pm(k)$ and $\hat{S}_{A,B}^{\pm}$ into the linearized gap equation, given in Eq. (2.18), one obtains the stability matrix as

$$\begin{aligned} \hat{M}_{a,b}^0 = \Gamma_a \sum_{kb} [& \\ & \cos(k\cdot a - \phi_k)\cos(k\cdot b - \phi_k) \left(\frac{\tanh\left(\frac{\beta\xi_+(k)}{2}\right)}{2\xi_+(k)} + \frac{\tanh\left(\frac{\beta\xi_-(k)}{2}\right)}{2\xi_-(k)} \right) \\ & + \sin(k\cdot a - \phi_k)\sin(k\cdot b - \phi_k) \frac{\sinh(\beta\mu)}{2\mu\cosh\left(\frac{\beta\xi_+(k)}{2}\right)\cosh\left(\frac{\beta\xi_-(k)}{2}\right)} \Bigg] \end{aligned} \tag{B3}$$

This is the same result obtained in Refs. [11, 20]. Let $f = M_{a,a}^0$ and $g = M_{a,b\neq a}^0$, then

$$\hat{M}_{a,b}^0 = \begin{pmatrix} f & g & g \\ g & f & g \\ g & g & f \end{pmatrix}. \tag{B4}$$

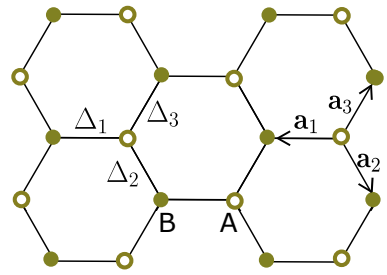

Figure B1. Schematic of the honeycomb lattice showing sublattices A (circle) and B (filled circle), the bond direction vector $(\mathbf{a_1}, \mathbf{a_2}, \mathbf{a_3})$ and bond dependent order parameter $\Delta = (\Delta_1 \ \Delta_2 \ \Delta_3)$.

$\hat{M}^0_{a,b}$ is a 3×3 matrix because there are three nearest-neighbor bond directions, with bond vectors $a = \left(a_1\, a_2\, a_3\right)$, in the honeycomb lattice, see figure B1. Therefore, the order parameter is bond dependent and has three components one along each bond direction. The gap the symmetries of the superconducting states are obtained by diagonalizing $\hat{M}^0_{a,b}$. The eigenvalues, eigenvectors, and their respective superconducting states are,

Eigenvalues	$f-g$	$f-g$	$f+2g$
Eigenvectors	$\frac{1}{\sqrt{6}}\left(2\ -1\ -1\right)^T$	$\frac{1}{\sqrt{2}}\left(0\ 1\ -1\right)^T$	$\frac{1}{\sqrt{3}}\left(1\ 1\ 1\right)^T$,
Superconducting states	$d_{x^2-y^2}$	d_{xy}	s_{ext}

where the top row are the eigenvalues, the second row are the corresponding eigenvectors, Δ_a and the third row superconducting states corresponding to each eigenvector in the D_{6h} point group.

The eigenvectors give the symmetry factors of the superconducting order parameter, as discussed in section 2.5.3. Then, the bond dependent nearest-neighbor superconducting order parameter can be collated as vector $\Delta = \Delta_0 \Delta_a = \left(\Delta_1 \Delta_2 \Delta_3\right)$, where Δ_0 is the strength of the pairing, see figure B1. Using the eigenvectors, Δ_a, as bond form factors for the superconducting pairing in momentum space, then expanding around a high symmetry point, the basis functions are obtained. The basis functions are then compared with the basis functions of the irreducible representations of D_{6h} point group, the determine the irreducible representation and symmetry of the superconducting state. The degenerate states are nodal d-waves belonging to the E_{2g} irreducible representation while fully symmetric state is the extended s-wave state belonging to the A_{1g} irreducible representation of D_{6h} point group, see Table 2.1.

As discussed in section 2.5.3, group theory allows for mixing of degenerate basis functions below T_c. In graphene it follows that equal mixing of the d-waves is favored below T_c form chiral d-wave, $d_{x^2-y^2} + id_{xy}$ superconducting

state with symmetry factors $\frac{1}{\sqrt{3}}\left(1, e^{i2\pi/3}, e^{-i2\pi/3}\right)^T$. Several theoretical studies, including mean-field [11, 20], renormalization group [13] and functional renormalization group [12], have predicted the existence of chiral d-wave superconductivity in honeycomb lattice at doping levels close to the van Hove singularity.

Appendix C.
Using projection operator to find basis functions

Using projection operator to find basis function

Define symmetry operations operator (or matrices) , P_R

- Rotation operations

In[976]:=
```
Rn[θ_] := RotationMatrix[θ, {0, 0, 1}];
(*Rotation along the principal axis which is along z*)
Rx[θ_] := RotationMatrix[θ, {1, 0, 0}]; (*Rotation along x-axis*)
C2' = Rx[π];
Ry[θ_] := RotationMatrix[θ, {0, 1, 0}]; (*Rotation along y-axis*)
C2'' = Ry[π];
```

```
Check rotation operations →
 {Rn[θ] // MatrixForm , C2' // MatrixForm, C2'' // MatrixForm}  →
  {( Cos[θ]  -Sin[θ]  0 )
   ( Sin[θ]   Cos[θ]  0 )
   (   0        0     1 ), ( 1  0  0 )
                            ( 0 -1  0 )
                            ( 0  0 -1 ), ( -1  0  0 )
                                         (  0  1  0 )
                                         (  0  0 -1 )}
```

- Reflection operations

In[982]:=
```
σd = ReflectionMatrix[{1, 0, 0}];
σv = ReflectionMatrix[{0, 1, 0}];
σh = ReflectionMatrix[{0, 0, -1}];
```

```
Check reflection operations →
 {σd // MatrixForm , σv // MatrixForm, σh // MatrixForm} →
  {( -1  0  0 )
   (  0  1  0 )
   (  0  0  1 ), ( 1  0  0 )
                 ( 0 -1  0 )
                 ( 0  0  1 ), ( 1  0  0 )
                              ( 0  1  0 )
                              ( 0  0 -1 )}
```

- Improper rotation operations

In[985]:=
```
Sn[θ_] := RotationMatrix[θ, {0, 0, 1}].σh →
 ( Cos[θ]  -Sin[θ]  0 )
 ( Sin[θ]   Cos[θ]  0 )
 (   0        0    -1 )
```

- Inversion operation

In[991]:=
```
invI = -IdentityMatrix[3];
```

Transformation function for symmetry operations, P_R^{Γ}

In[986]:=
```
opRule[O_] := Thread[{x, y, x} → O.{x, y, z}];
```

Note that this P_R^{Γ} the projection of each symmetry element under the irreducible representation Γ. Summing all P_R^{Γ} gives the projection operator

Eq. (2.26) i.e. $P^{\Gamma} = \Sigma_R P_R^{\Gamma}$.

opRule takes in P_R and then aplies it on coordinates {x, y, z} transforming it to new coordinates {x1, y1, z1}

In[987]:=
```
Test the function → opRule[Rn[2 π / 6]] // MatrixForm; →
```
$$\begin{pmatrix} x \to \frac{x}{2} - \frac{\sqrt{3}\,y}{2} \\ y \to \frac{\sqrt{3}\,x}{2} + \frac{y}{2} \\ z \to z \end{pmatrix}$$

Finding basis functions of D_{6h} using the projection operator

As an example consider two arbitrary functions basis1 = $x^2 + y^2$ and basis2 = $x^2 - y^2$, the task is to check if these functions are basis functions of A_{1g} or E_{2g}. Using Eq. (3.1) in the main text one finds the irreps to which the basis function belongs to as follows :

In[989]:=
```
basis1 = x^2 + y^2;  basis2 = x^2 - y^2;
```

[g] = 24; dim [A_{1g}] = 1; dim [E_{2g}] = 2;

The characters χ and number of elements in a class, N_k are read from Table 3.1

- Try basis1 under A_{1g}

In[994]:=
```
A1gBasis1 = Simplify[
  1/24 ((1) (1) (basis1 /. opRule[Rn[0]]) + (1) (2) (basis1 /. opRule[Rn[2 π / 6]]) +
    (1) (2) (basis1 /. opRule[Rn[2 π / 3]]) +
    (1) (1) (basis1 /. opRule[Rn[2 π / 2]]) + (1) (3) (basis1 /. opRule[C2']) +
    (1) (3) (basis1 /. opRule[C2'']) + (1) (1) (basis1 /. opRule[invI]) +
    (1) (2) (basis1 /. opRule[Sn[2 π / 6]]) +
    (1) (2) (basis1 /. opRule[Sn[2 π / 3]]) + (1) (1) (basis1 /. opRule[σh]) +
    (1) (3) (basis1 /. opRule[σv]) + (1) (3) (basis1 /. opRule[σd]))]
```

```
x^2 + y^2 → x^2 + y^2 is a basis function of A1g
```

- Try basis2 under A_{1g}

In[995]:=
```
A1gBasis2 = Simplify[
  1/24 ((1) (1) (basis2 /. opRule[Rn[0]]) + (1) (2) (basis2 /. opRule[Rn[2 π / 6]]) +
    (1) (2) (basis2 /. opRule[Rn[2 π / 3]]) +
    (1) (1) (basis2 /. opRule[Rn[2 π / 2]]) + (1) (3) (basis2 /. opRule[C2']) +
    (1) (3) (basis2 /. opRule[C2'']) + (1) (1) (basis2 /. opRule[invI]) +
    (1) (2) (basis2 /. opRule[Sn[2 π / 6]]) +
    (1) (2) (basis2 /. opRule[Sn[2 π / 3]]) + (1) (1) (basis2 /. opRule[σh]) +
    (1) (3) (basis2 /. opRule[σv]) + (1) (3) (basis2 /. opRule[σd]))]
```

```
1/2 (x^2 - y^2) → x^2 - y^2 is not a basis function of A1g
```

- Try basis1 under E_{2g}

In[996]:=
```
E2gBasis1 = Simplify[
  2/24 ((1) (2) (basis1 /. opRule[Rn [0]]) + (2) (-1) (basis1 /. opRule[Rn [2 π / 6]]) +
     (2) (-1) (basis1 /. opRule[Rn [2 π / 3]]) +
     (1) (2) (basis1 /. opRule[Rn [2 π / 2]]) + (3) (0) (basis1 /. opRule[C2']) +
     (3) (0) (basis1 /. opRule[C2'' ]) + (1) (2) (basis1 /. opRule[invI]) +
     (2) (-1) (basis1 /. opRule[Sn [2 π / 6] ]) +
     (2) (-1) (basis1 /. opRule[Sn [2 π / 3] ]) + (1) (2) (basis1 /. opRule[σh]) +
     (3) (0) (basis1 /. opRule[σv]) + (3) (0) (basis1 /. opRule[σd]))]
```

```
0 → x^2 + y^2 not a basis function of E2g
```

- Try basis2 under E_{2g}

In[997]:=
```
E2gBasis2 = Simplify[
  2/24 ((1) (2) (basis2 /. opRule[Rn [0]]) + (2) (-1) (basis2 /. opRule[Rn [2 π / 6]]) +
     (2) (-1) (basis2 /. opRule[Rn [2 π / 3]]) +
     (1) (2) (basis2 /. opRule[Rn [2 π / 2]]) + (3) (0) (basis2 /. opRule[C2']) +
     (3) (0) (basis2 /. opRule[C2'' ]) + (1) (2) (basis2 /. opRule[invI]) +
     (2) (-1) (basis2 /. opRule[Sn [2 π / 6] ]) +
     (2) (-1) (basis2 /. opRule[Sn [2 π / 3] ]) + (1) (2) (basis2 /. opRule[σh]) +
     (3) (0) (basis2 /. opRule[σv]) + (3) (0) (basis2 /. opRule[σd]))]
```

```
x^2 - y^2 → x^2 - y^2 is a basis function of E2g
```

In[967]:=
```
Export["ProjectionOperatorD6h.pdf", EvaluationNotebook[]]
```

Out[967]=
```
ProjectionOperatorD6h.pdf
```

Acta Universitatis Upsaliensis

Digital Comprehensive Summaries of Uppsala Dissertations from the Faculty of Science and Technology 2047

Editor: The Dean of the Faculty of Science and Technology

A doctoral dissertation from the Faculty of Science and Technology, Uppsala University, is usually a summary of a number of papers. A few copies of the complete dissertation are kept at major Swedish research libraries, while the summary alone is distributed internationally through the series Digital Comprehensive Summaries of Uppsala Dissertations from the Faculty of Science and Technology. (Prior to January, 2005, the series was published under the title "Comprehensive Summaries of Uppsala Dissertations from the Faculty of Science and Technology".)

Distribution: publications.uu.se
urn:nbn:se:uu:diva-440982

ACTA
UNIVERSITATIS
UPSALIENSIS
UPPSALA
2021